

UC Santa Cruz

UC Santa Cruz Electronic Theses and Dissertations

Title

The Neuroprotective Self-Regulation of the Prion Protein is Driven by Copper Coordination to Both C and N-Terminal Histidines, and is Refined by Glycans

Permalink

<https://escholarship.org/uc/item/6qx2d2bh>

Author

Schilling, Kevin

Publication Date

2021

Peer reviewed|Thesis/dissertation

UNIVERSITY OF CALIFORNIA
SANTA CRUZ

**The Neuroprotective Self-Regulation of the Prion Protein is Driven by Copper
Coordination to Both C and N-Terminal Histidines, and is Refined by Glycans**

A dissertation submitted in partial satisfaction
of the requirements for the degree of

DOCTOR OF PHILOSOPHY

in

CHEMISTRY

by

Kevin C. M. Schilling

December 2021

The Dissertation of Kevin C. M. Schilling
is approved:

Professor Seth M. Rubin, chair

Professor Glenn L. Millhauser

Professor Jevgenij A. Raskatov

Peter Biehl
Vice Provost and Dean of Graduate Studies

Copyright © by
Kevin C. M. Schilling
2021

Table of Contents

Chapter 1. Introduction	1
Chapter 2. Both N-Terminal and C-Terminal Histidine Residues of the Prion Protein are Essential for Copper Coordination and Neuroprotective Self-Regulation	6
Introduction	7
Results	10
Discussion	27
Materials and Methods	32
Acknowledgements	39
Supporting Information	40
Chapter 3. Production of Artificially Doubly Glycosylated, ¹⁵N Labelled Prion Protein for NMR Studies Using a pH-Scanning Volatile Buffer System ..	43
Introduction and Results	44
Materials and Methods	49
Acknowledgements	52
Supporting Information	53
Chapter 4. The Prion Protein's Glycans Refine its Neuroprotective, Copper-Driven Self-Regulatory <i>Cis</i> Interaction	60
Introduction	61
Results	63
Discussion	68

Materials and Methods	69
Acknowledgements	71
Chapter 5. Conclusion	72
References	76

List of Figures

Chapter 2

Figure 1: Current understanding of prion protein structure	9
Figure 2: Effects of histidine mutation on paramagnetic relaxation effect derived line broadening	14
Figure 3: Movement of histidine along C-terminal alpha helix prompts copper to follow	16
Table 1: Summary of couplings from EPR experiments and their meanings	19
Figure 4: EPR experiments comparing wild-type PrP ^C with H139Y, H176Y mutant PrP ^C	20
Figure 5: Effects of octarepeat histidine insertion mutations on paramagnetic relaxation effect derived line broadening	22
Figure 6: Electrophysiology experiments on mutants of the prion protein	24
Figure 7: A structural explanation for the results of chapter 1	31
Table 2: Constructs tested by NMR in chapter 1	33
Supporting Figure 1: Comparison of peak intensity reduction in wild-type and H139Y, H176Y mutant PrP ^C	40
Supporting Figure 2: Central region histidines 95 and 110 are not involved in copper binding at pH 6	41
Supporting Figure 3: NMR spectra of mutant PrP ^C with and without copper	41
Supporting Figure 4: Interaction strengthened when one octarepeat histidine deleted	42

Chapter 3

Figure 1: Mechanism of pH-scanning volatile buffer	46
Figure 2: pH as a function of time for pH scanning buffer	47
Figure 3: Synthesis scheme for artificially glycosylated PrP ^C	48
Supporting Figure 1: LCMS spectra of ¹⁵ N wild-type PrP ^C with <i>p</i> -Acetyl-phenylalanine at positions 180 and 196	53
Supporting Figure 2: LCMS spectra of ¹⁵ N wild-type PrP ^C with one-sugar-long glycans at positions 180 and 196	54
Supporting Figure 3: LCMS spectra of ¹⁵ N wild-type PrP ^C with two-sugar-long glycans at positions 180 and 196	55
Supporting Figure 4: LCMS spectra of ¹⁵ N wild-type PrP ^C with three-sugar-long glycans at positions 180 and 196	56
Supporting Figure 5: ¹ H- ¹⁵ N HSQC NMR of wild-type PrP ^C and wild-type PrP ^C with three-sugar-long glycans at positions 180 and 196	57
Supporting Figure 6: CD spectra of wild-type and glycomimetic PrP ^C	57
Supporting Figure 7: Raw data of buffer pH vs time for various buffer concentrations, with and without stirring	58
Supporting Figure 8: Change in pH over time of volatile buffer mixtures	59

Chapter 4

Figure 1: Continuous wave EPR spectra showing the copper coordination environment in glycosylated and unglycosylated PrP ^C	63
---	----

Figure 2: Surface representations showing areas of wild-type PrP ^C engaged in the <i>cis</i> interaction, with and without glycans	65
Figure 3: Surface representation showing the areas of wild-type PrP ^C engaged in the <i>cis</i> interaction that change the most with the addition of glycans	66
Figure 4: Surface representations showing areas of H139Y, H176Y PrP ^C engaged in the <i>cis</i> interaction, with and without glycans	68
Chapter 5	
Figure 1: Unified model showing three contributors to the <i>cis</i> interaction in PrP ^C	75

Abstract

The Neuroprotective Self-Regulation of the Prion Protein is Driven by Copper Coordination to Both C and N-Terminal Histidines, and is Refined by Glycans

Kevin C. M. Schilling

The cellular prion protein (PrP^C) is comprised of two domains – a globular C-terminal domain and an unstructured N-terminal domain. Copper drives tertiary contact in PrP^C, inducing a neuroprotective *cis* interaction that structurally links the protein's two domains. The location of this interaction on the C-terminus overlaps with the sites of human pathogenic mutations and toxic antibody docking. Combined with recent evidence that the N-terminus is a toxic effector regulated by the C-terminus, there is an emerging consensus that this *cis* interaction serves a protective role, and that the disruption of this interaction by misfolded PrP oligomers may be a cause of toxicity in prion disease. We demonstrate here that two highly conserved histidines in the C-terminal domain of PrP^C are essential for the protein's *cis* interaction, which helps to protect against neurotoxicity carried out by its N-terminus. We show that simultaneous mutation of these histidines drastically weakens the *cis* interaction and enhances spontaneous cationic currents in cultured cells - the first C-terminal mutant to do so. Whereas previous studies suggested that Cu²⁺ coordination was localized solely to the protein's N-terminal domain, we find that both domains contribute equatorially coordinated histidine residue side chains, resulting in a novel bridging interaction. We also find that extra N-terminal histidines in pathological familial mutations involving

octarepeat expansions inhibit this interaction by sequestering copper from the C-terminus. Our findings further establish a structural basis for PrP^C's C-terminal regulation of its otherwise toxic N-terminus.

The glycans of the prion protein are located in close proximity to the C-terminal histidines that we have shown are necessary for the neuroprotective copper tether. The recombinant protein used for the previously described experiments lacked glycans, and we wondered if they would have any effect on the observed interaction. Since the glycans are fairly large and located on the surface of the protein, we thought that they may sterically hinder the *cis* interaction, falsifying or requiring modification of the interpretation of the previously described results. We set out to create glycosylated protein in order to directly test the impact of these moieties on the protective *cis* interaction.

Bacterially expressed proteins used in NMR studies lack glycans, and proteins from other organisms are neither ¹⁵N labelled, nor glycosylated homogeneously. We developed a method to add two artificial glycans to uniformly ¹⁵N labelled prion protein, using a buffer system that evolves over a pH range in order to accommodate the conflicting pH requirements of the substrate and enzymes, without the need to fine tune buffer conditions. NMR and CD spectroscopy of the protein indicates that the glycans do not influence its fold.

Using our glycosylated, ¹⁵N labelled protein, we tested the effects of the glycans on the protein's previously observed *cis* interaction. In opposition to our hypothesis that the glycans would prevent the interaction through steric hindrance, we observed

that the interaction was refined by the glycans; the glycans narrow down the region of the C-terminus with which copper interacts. We then found that the presence of glycans partially restores the lost *cis* interaction observed when C-terminal histidines are mutated away.

Together, the work in this dissertation shows that both N and C-terminal histidines of the prion protein bind copper ions, driving a neuroprotective self-regulatory interaction, and that the glycans of the protein refine and strengthen this interaction.

Acknowledgements

This research was made possible by a supportive group of mentors, coworkers, and collaborators. My Ph.D. advisor, professor Glenn Millhauser, kept his office door open, balanced support with experimental freedom, and secured funding for this research. My dissertation committee members, professors Seth Rubin and Jevgenij Raskatov, provided valuable scientific advice during and after my qualifying exam. Jack Lee, the Director of NMR Technology at UCSC, provided hands on training and assistance for many of the experiments presented in this dissertation.

In addition to support given by mentors here at UCSC, the efforts of external collaborators also enabled this work. Professor David Harris and his student Bei Wu at Boston University conducted electrophysiology experiments that demonstrated the importance of our central findings. Professor David Britt and his student Lizhi Tao at UC Davis conducted electron paramagnetic resonance experiments that clarified our findings. Dr. Jake Pushie at the University of Saskatchewan conducted computational simulations that reinforced our findings.

The other graduate students in the Millhauser lab contributed in various ways to this work. Valerie Chen is an outside the box thinker who is perfect for talking through scientific ideas with, and she directly suggested some of the experiments presented in this dissertation. Graham Roseman is a human library who mentored me during my rotation in the Millhauser lab and suggested the starting point for this project. Kate Markham is a great scientist with an objective outlook and no appetite for

sugarcoating information, which makes her a very useful friend to have. Francesca Pavlovici is always looking out for other people and catalyzes interactions.

The postdocs in the Millhauser lab, Drs. Tufa Assafa and Scarlett Dvorkin, assisted with spectroscopy experiments. I had the pleasure to mentor a few undergraduate students – Joseph Kiblen, Natalia Ubilla-Rodriguez, and Conner Wells, who were all extremely motivated and hard working.

This research was also made possible by contributions from the taxpayer, administered through the National Institutes of Health.

The text of this dissertation includes reprints of the following previously published material:

1) Kevin M. Schilling, Lizhi Tao, Bei Wu, Joseph T.M. Kiblen, Natalia C. Ubilla-Rodriguez, M. Jake Pushie, R. David Britt, Graham P. Roseman, David A. Harris, Glenn L. Millhauser. Both N-Terminal and C-Terminal Histidine Residues of the Prion Protein Are Essential for Copper Coordination and Neuroprotective Self-Regulation. *Journal of Molecular Biology* **2020**, 432, 16, 4408-4425.

2) Kevin M. Schilling, Natalia C. Ubilla-Rodriguez, Conner W. Wells, and Glenn L. Millhauser. Production of Artificially Doubly Glycosylated, ¹⁵N Labeled Prion Protein for NMR Studies Using a pH-Scanning Volatile Buffer System. *Journal of Organic Chemistry* **2019**, 85, 3, 1687-1690.

The co-authors Glenn L. Millhauser, David A. Harris, and R. David Britt directed and supervised the research which forms the basis for the dissertation. The co-author Lizhi Tao performed the EPR experiments in chapter 2. The co-author Bei Wu performed the electrophysiology experiments in chapter 2. The co-author Jake Pushie performed the molecular dynamics and DFT experiments in chapter 2. The co-authors Joseph T.M. Kiblen, Natalia C. Ubilla-Rodriguez, and Conner W. Wells assisted with various experiments in chapters 2 and 3. Dr. Tufa Assafa performed the EPR experiments in chapter 4.

Chapter 1
Introduction

Introduction

Prion diseases, or Transmissible Spongiform Encephalopathies (TSEs), are a class of contagious, fatal neurodegenerative illnesses brought on by the misfolding of the endogenous prion protein (PrP) [1,2]. These diseases, which are part of a larger group of protein aggregation disorders including Alzheimer's and Parkinson's diseases, are an ongoing threat to human health, as well as to agricultural and wildlife animals.

Prion diseases are initiated by the misfolding of the prion protein (PrP) from its cellular form (PrP^C) into a beta sheet rich form (PrP^{Sc}) [1,2]. Misfolded PrP^{Sc} aggregates usually deposit as fibrillar structures in brain tissue. The self-propagating nature of these aggregates has been extensively studied[2-4], but the mechanism of their neuronal toxicity is still unknown. PrP null mice do not exhibit symptoms of prion disease, suggesting that the disease is due to the gain of a toxic function, rather than the loss of essential activity[5]. PrP null mice injected with PrP^{Sc} do not show symptoms of prion disease, demonstrating the requirement of PrP^C as an essential precursor to PrP^{Sc}. In addition, PrP^C has been implicated as a signal transducer that transmits the toxicity initiated by PrP^{Sc}[6-9].

Several kinds of experiments suggest that alterations in PrP^C structure or conformation may mediate neurotoxic activities. For example, expression in transgenic mice of PrP sequences harboring deletions within the central domain of PrP, such as Δ 105-125, causes a spontaneous neurodegenerative phenotype. In addition, monoclonal antibodies that bind the C-terminal domain of PrP^C are profoundly neurotoxic *in vivo* and in cultured cells[10-12]. It is thought that these manipulations

eliminate the necessity for PrP aggregation, and directly induce PrP^C-mediated neurodegeneration. The effects of PrP deletions and anti-PrP antibodies can be measured in cell culture using patch-clamp recording, which detects the spontaneous, cationic currents[13].

In electrophysiological assays and *in vivo*, it has been observed that the flexible N-terminal domain, and in particular the first nine residues (23-31), are essential for neurotoxic activity[11,14]. Deletion of these residues, or treatment with antibodies and other ligands that bind this region, prevents the spontaneous currents and other neurotoxic activities[12,14]. In addition, cells expressing the N-terminal domain of PrP attached to another protein, EGFP, and entirely devoid of the C-terminal domain of PrP, exhibit spontaneous currents[11]. These results suggest that the N-terminal domain of PrP harbors a latent, toxic effector action, which is normally inhibited by interaction with the C-terminal domain.

The specific region on the C-terminus of PrP^C where toxic antibodies bind is near the sites of pathogenic, familial mutations[15,16]. Recently, our lab and others have shown that there is a *cis* interaction between the N-terminal and C-terminal domains of PrP^C, and that disruption of this interaction leads to neurotoxicity[15,17,18]. Taken together, these results suggest that an unregulated N-terminal domain of PrP^C is responsible for neurotoxicity, and that toxic PrP oligomers (ranging in size from ~5-10 PrP units[19,20]) may interfere with a natural protective regulation of the N-terminal domain by the C-terminal domain[11,18]. Despite the importance of PrP^C's self-regulation, only limited information is known about the

essential regulatory interface between the two domains, although important insights have recently come from a study using a combination of cross-linking mass spectrometry and NMR[21].

In order to understand the molecular details of PrP^C's self-regulation, we consider the role of the protein's cognate metal ions. PrP physiology is highly dependent on the concentrations of divalent metal ions, particularly Cu²⁺. PrP has been shown to concentrate copper in brain tissue, and its expression is upregulated in response to copper binding to the *PNRP* promoter [22-24]. PrP is also known to regulate ion channels in a copper dependent manner[6,25]. Due to the strong link between copper and PrP function, the metal binding properties of the protein have been extensively studied[15,18,26-32]. In the N-terminus of the protein, there is a tandem eight amino acid sequence repeated four times (octarepeat, OR; Figure 1). Each repeat contains one histidine, capable of coordinating the divalent metal ions Cu²⁺ and Zn²⁺. Cu²⁺ is found to bind the four histidine residues in the N-terminal domain's octarepeat region with sub-nanomolar affinity[29].

N-terminal copper binding has been observed to drive tertiary structure in PrP^C, inducing the aforementioned *cis* interaction between the N- and C-terminal domains of the protein[15,17,18,21]. The location of this interaction on the C-terminus overlaps with the sites of pathogenic mutations and toxic antibody docking. Copper delivered to cells has been shown to partially rescue toxicity resulting from deletion of a hydrophobic segment between the PrP^C N- and C-terminal domains[11]. Together, these results suggest that PrP^C's neuroprotective self-regulation is in fact driven by

copper, which directly promotes the *cis* interaction between its toxic N-terminal and regulatory C-terminal domains.

The region on the C-terminus in which N-terminally bound copper has been observed to localize is nearby two highly conserved histidines, as well as the protein's glycans[15,17,18]. The first body chapter in this dissertation investigates the link between these C-terminal histidines and the *cis* interaction. We found that these histidines coordinate copper simultaneously with N-terminal histidines, forming a tether between the two termini of the protein. Removal of these histidines inhibits the *cis* interaction, and leads to toxic spontaneous currents in cell culture – a sign of prion-like toxicity. We use these findings to propose a mechanism of action for a class of genetic prion diseases – the octarepeat deletion disorders, and show NMR data supporting this claim. The second chapter is the creation of a method to prepare ¹⁵N labelled, homogenously artificially glycosylated PrP^C, which is necessary for NMR studies on the effects of the glycans. As a sub development, we create a volatile, pH-scanning buffer that allows us to sample a spectrum of reaction conditions automatically. The third chapter in this dissertation is a set of NMR and EPR experiments, which show that the prion protein's glycans refine the *cis* interaction; the glycans narrow the region of the C-terminus with which copper interacts. We also found that the presence of glycans partially restores the lost *cis* interaction observed when C-terminal histidines are mutated away. In summary, we found that C-terminal histidines and glycans both play a role in a neuroprotective self-regulation of the prion protein, and suggest that their absence can lead to diseased states.

Chapter 2

Both N-Terminal and C-Terminal Histidine Residues of the Prion Protein are Essential for Copper Coordination and Neuroprotective Self-Regulation.

Kevin M. Schilling^a, Lizhi Tao^b, Bei Wu^c, Joseph T.M. Kiblen^a, Natalia C. Ubilla-Rodriguez^a, M. Jake Pushie^d, R. David Britt^b, Graham P. Roseman^a, David A. Harris^{*c}, and Glenn L. Millhauser^{*a}

^a 1156 High Street. Department of Chemistry and Biochemistry, University of California, Santa Cruz, CA, 95064, United States

^b 1 Shields Ave. Department of Chemistry, University of California, Davis, CA, 95616, United States

^c 72 E. Concord St Silvio Conte. Department of Biochemistry, Boston University School of Medicine, Boston, MA, 02118, United States

^d 107 Wiggins Rd B419. Department of Surgery, College of Medicine, University of Saskatchewan, Saskatoon, SK S7N 5E5, Canada

Introduction

Copper bound to the N-terminus of the prion protein drives a *cis* interaction in the protein – the N and C termini are brought together to form a neuroprotective self-regulatory structure. How does copper cause the two domains to co-localize? Upon examination of the region on the C-terminus of PrP^C in which the copper-bound N-terminus docks, we were struck by the presence of two highly conserved histidine residues (Figure 1). The goal of this study is to determine if these C-terminal histidines facilitate the interdomain *cis* interaction, perhaps by acting as a tether to hold the two domains together. If so, a paradox is presented: if the copper ion is already coordinatively saturated by four N-terminal histidines, how could it bind additional C-terminal histidines?

To investigate a potential role of C-terminal histidines in the prion protein's *cis* interaction, we employed ¹H-¹⁵N HSQC NMR analysis of the murine protein. We show that mutation of histidines 139 and 176 (equivalent to human residues 140 and 177) results in a drastic weakening of the *cis* interaction. Furthermore, when His176 is deleted and a new histidine is added one turn up or down on the same helix, the location of the *cis* interaction tracks the position of the histidine. We propose a model for this interaction in which copper acts as a tether – being simultaneously bound by both N and C-terminal histidine residues, analogous to the Cu(II) macro-chelate that occurs between His50 and Asp2 of α -Synuclein[33]. Using EPR spectroscopy, we find that the mechanism of this tether involves a histidine swap – one N-terminal histidine is removed from the copper ion and replaced with a C-terminal histidine. We show this

model to be energetically plausible using molecular dynamics simulations and supporting density functional structure calculations. Together, these findings overturn the conventional view that Cu^{2+} is bound solely to the PrP^C N-terminal domain. Instead, both domains participate in metal ion coordination.

We find that, in addition to its structural effects, disruption of the *cis* interaction by mutation of both C-terminal histidines H139 and H176 enhances spontaneous ionic currents in cultured cells – the first C-terminal mutant to do this. Lastly, we find that the insertional mutations of extra, histidine containing octarepeat segments, which are linked to familial prion diseases, inhibit the protein's *cis* interaction by chelating copper away from the C-terminus. These findings advance our understanding of the toxicity caused by prion oligomers, toxic antibodies, and pathological mutations, and suggest that strengthening the *cis* interaction may be an effective therapeutic strategy for prion disease.

Results

Mutation of histidines 139 and 176 drastically weakens the prion protein's *cis* interaction

To examine whether C-terminal histidines contribute to the *cis* interaction, we mutated histidines 139, 176, and 186 of the murine prion protein to tyrosine, each in separate mutants. Because His186 is on the opposite face of the protein from the site of the *cis* interaction, we included it as a control. We chose tyrosine as a replacement amino acid because it is structurally similar to histidine, but cannot bind metals with similar affinity. At pH 7.4, the N-terminus of PrP^C binds copper in three coordination modes[26,27,29]. At low copper : PrP^C ratios, one copper ion is bound simultaneously by four histidines from the octarepeat region of PrP^C. At higher copper levels, multiple copper ions bind to the protein. In order to simplify interpretation of the data, we performed our experiments at pH 6.0, which locks the coordination into the first mode. Using ¹H-¹⁵N HSQC NMR at 37 °C and pH 6.0, we measured the peak intensities of C-terminal residues with no copper, and with one equivalent CuCl₂. Dividing the intensity of each peak in the copper sample by its corresponding intensity in the apo sample, we calculated the intensity ratios (i/i_0) associated with the addition of one equivalence of copper to the protein, and repeated this process for each mutant. We then scaled the i/i_0 values to eliminate the effects of differential unspecific peak intensity reduction across mutants, and mapped the results onto the surface of the three-dimensional structure of the protein's helical C-terminus.

The wild-type protein showed peak intensity reduction due in part to the paramagnetic relaxation effect (PRE), and also to exchange, in three areas as reported previously[17,18]. We refer to these areas of the helical C-terminal domain as “patch 1”, which is centered around His139, “patch 2”, which is centered around His176, and “patch 3”, which is located on helix three, between patch 1 and patch 2 (Figure 2). The peak intensity reduction in patches 1 and 2 is stronger than in patch 3, suggesting that they are closer to the bound copper center of the OR. The H139Y mutation resulted in a much weaker peak intensity reduction at patch 1 than wild type, as did the H176Y mutation but at patch 2, while the H186Y mutation did not result in a difference to peak intensity reduction. The mutation of H186, which is the location of the pathogenic mutation H186R, appeared to affect C-terminal conformation of the protein and was therefore not further investigated. We varied protein and copper concentrations to test for the possibility of intermolecular interactions. We found that the peak linewidths were invariant as a function of protein concentration. In addition, the i/i_0 profiles were not affected as would be expected if two PrP^C molecules were forming a complex at higher concentrations. Together, these results suggest that there is only one PrP^C molecule involved per copper, and that the interaction is strictly between its N and C termini.

With the mutation of only one C-terminal histidine at a time, the *cis* interaction persisted, centered around the remaining histidine. We then made the double mutant (H139Y,H176Y), to test the theory that either histidine was capable of driving the interaction. In this mutant we observed that both patches 1 and 2 exhibited significantly

decreased peak intensity reduction compared to wild type, abolishing the primary contacts of the established *cis* interaction (Figure 2). Peak intensity in patch 3 was also slightly *more* reduced than in wild type, suggesting a backup, albeit weak, mode of *cis* interaction. The strength of this backup interaction is best visualized using the bar plot of peak intensity ratios in Figure 2. We note that residues N-terminal to residue 120 are largely unstructured, resulting in peak overlap that confounds extraction of peak intensities, and have not been included in this analysis.

In order to be sure that these effects were due to the removal of histidines, and not due to addition of tyrosines which could sterically hinder the *cis* interaction, we performed these same experiments with the mutants (H139N,H176N) and (H139A,H176A), and observed the same results (data not shown).

We also performed this experiment on 90-230 PrP^C, which lacks the octarepeat histidines, to check that the observed C-terminal peak intensity reduction was due to a *cis* interaction rather than pure C-terminal copper binding. Although we observed slight intensity reduction around the C-terminal histidines in this mutant, the effect was much weaker than in the full-length protein. This observation provides convincing evidence that the reduction in peak intensity observed in the wild-type protein upon the addition of copper results from the *cis*-interaction between its two domains, and not from transient copper binding solely to the C-terminal domain. Specifically, the loss of the octarepeat domain has a major effect on copper binding in the C-terminal domain, especially at His176.

Previous research by us and others has demonstrated the involvement of the non-octarepeat histidines H95 and H110 in copper binding[27,30,34]. At pH 7.4, copper coordination at these sites involves both the His side chain, as well as backbone amide nitrogens. To eliminate interference from coordination at these sites, we performed experiments at pH 6.0, which suppresses deprotonation of amides, thus reducing localized non-octarepeat copper binding. As a further control aimed at probing the involvement of histidines H95 and H110 in this interaction, we performed NMR on the construct (H95Y, H110Y). The strength and location of the *cis* interaction observed here is nearly identical to the wild-type protein (Figure S1). We also performed continuous wave EPR on the wild-type protein at both pH 6.0 and pH 7.4. In the pH 7.4 spectrum we observed a previously characterized signal that arises from copper coordination from His95 and His110 due to backbone protonation, but we do not see this coordination in the pH 6.0 spectrum (Figure S2). Based on this data, we can rule out the possibility that the C-terminus is interacting with copper bound solely to a central region histidine complex. However, we cannot rule out the possibility that the C-terminus is interacting with copper bound to a complex formed of both the octarepeat and central region histidines.

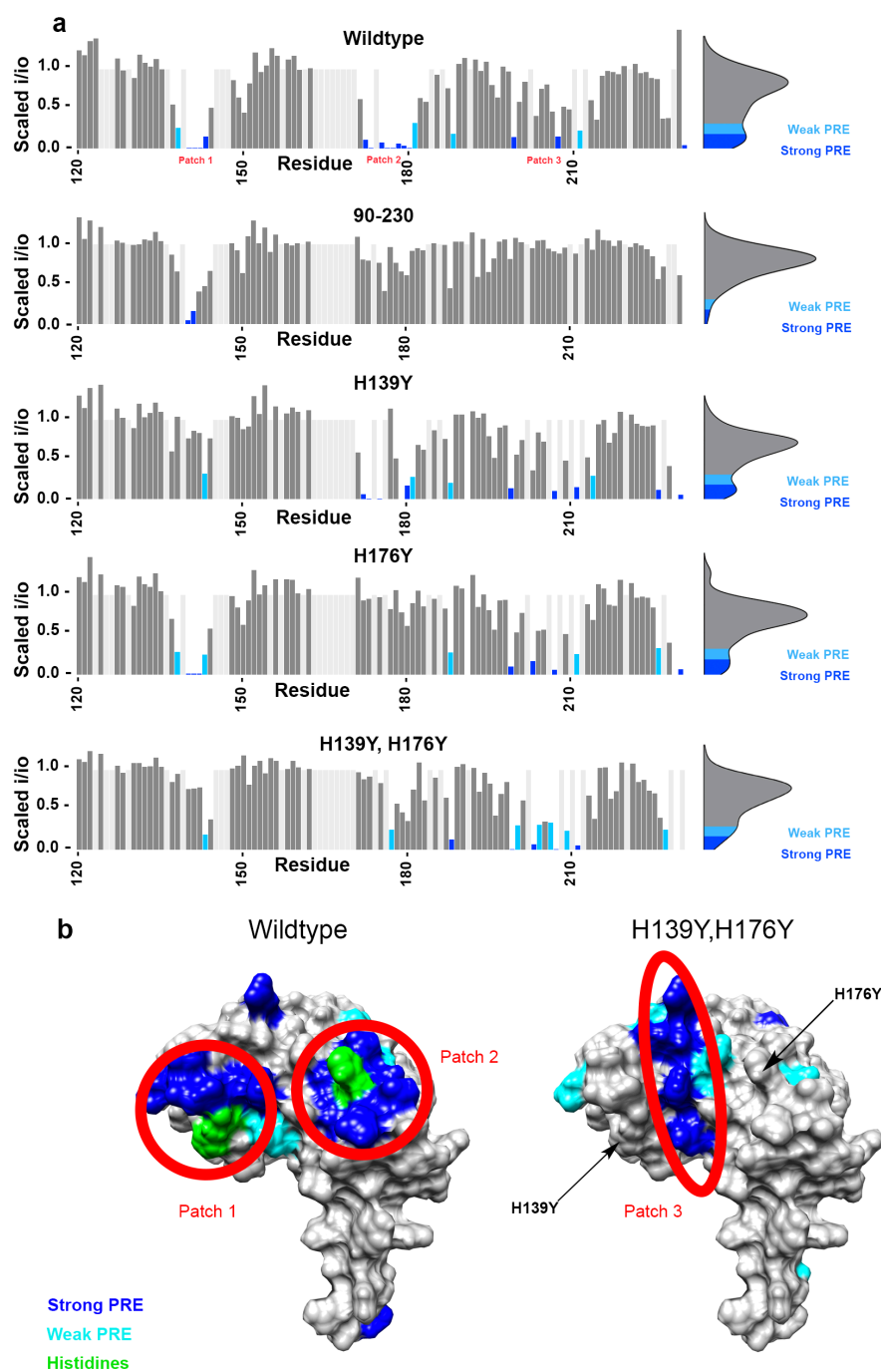


Figure 2. a) Bar plots showing the magnitude of the peak intensity reduction derived from the paramagnetic relaxation effect (PRE) on specific residues of the protein's C-terminal domain, with 1 equivalent of CuCl_2 at pH 6.0 in 10 mM MES buffer for all five protein samples. Patches 1 and 2, which are located around histidines 139 and 176 respectively, are much more strongly affected in the wild-type protein than in (H139Y,H176Y) and in 90-230 PrP^C. Unassigned residues are light grey and are drawn with no intensity reduction. **b)** Surface representations showing areas engaged in the *cis* interaction, as measured by the intensity reduction of NMR cross peaks, plotted on PDB: 1XYX.

Mutation of C-terminal residues in the region of the *cis* interaction surrounding histidines 139 and 176 does not abolish the interdomain interaction

In order to show that the *cis* interaction was driven by histidine-copper interactions rather than by a specific interaction between the two domains of the protein, we mutated most of the other residues in patches 1 and 2 spatially adjacent to the histidines to alanine. Specifically, the mutants (137A,138A,140A) and (172A,173A,175A,179A,180A) were created, as these are the residues that are located most closely to His139 and H176, and examined by NMR. The mutant (137A,138A,140A) adopted a misfold, preventing the data from being analyzed. The mutant (172A,173A,175A,179A,180A), which mutates the majority of patch 2 but leaves its histidine intact, maintained its i/i_0 profile consistent with the protein's *cis* interaction (Figure S3). These results reaffirm the importance of this C-terminal histidine in the copper driven *cis* interaction.

Deletion of histidine 176 and introduction of a new histidine one turn up or down its helix leads to a *cis* interaction localized to the new histidine

To show that the histidines were actively driving the *cis* interaction, rather than simply being positioned in the center of the involved areas, we deleted His176 and created two new mutants, one with a histidine one turn up and the other with a histidine one turn down its helix. As observed in Figure 3, the location of patch 2 follows the histidine. The ability of the histidine on helix 2 to control the location the *cis* interaction shows that it plays an active role in this docking event.

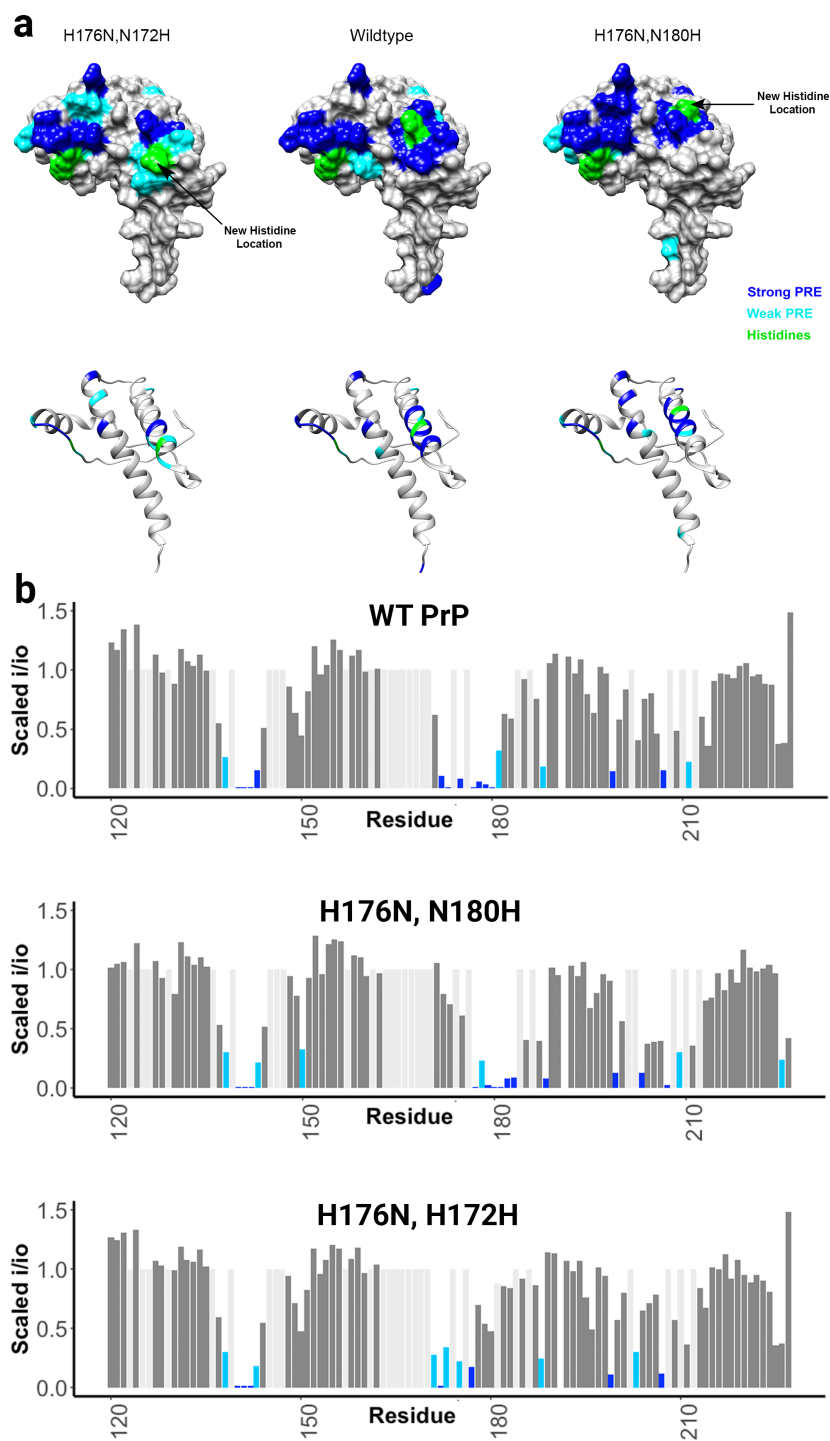


Figure 3: a) Surface representations showing areas engaged in the *cis* interaction, as measured by the intensity reduction of NMR cross peaks, plotted on PDB: 1XYX. This figure shows that the *cis* interaction follows histidine 176. **b)** Bar plots showing the magnitude of the peak intensity reduction derived from the paramagnetic relaxation effect (PRE) on specific residues of the protein's C-terminal domain, with 1 equivalent of CuCl_2 at pH 6.0 in 10 mM MES buffer for all protein samples.

Electron paramagnetic resonance (EPR) experiments show no change in copper coordination environment, suggesting an equatorial histidine swap

Copper(II) in aqueous solutions exists in octahedral or square planer coordination geometries. With the knowledge that the four histidines of the PrP^C N-terminal octarepeat domain bind copper equatorially, this leaves only the axial binding sites available for a fifth, C-terminal histidine ligand. To investigate the coordination environment of the copper center, we employed X-band continuous wave (CW) EPR, Q-band electron nuclear double resonance (ENDOR), and hyperfine sub-level correlation (HYSCORE) spectroscopy at pH 6 (Figure 4).

As shown in Figure 4A, WT and the double mutant (H139Y, H176Y), which we refer to as “DM,” produces the same X-band CW EPR spectra, which are well simulated by employing four equatorial nitrogen nuclei (^{15}N , $I = 1/2$) with a strong hyperfine coupling of a_{iso} ca. 55 MHz. This strong ^{15}N hyperfine coupling arises from directly coordinated nitrogens ($^{15}\text{N}_{\delta}$) of the equatorial His imidazole rings. The remote histidine nitrogens ($^{15}\text{N}_{\epsilon}$), that are two bonds away from the $^{15}\text{N}_{\delta}$, typically have a much smaller hyperfine coupling. This smaller coupling was probed by using Mims-ENDOR shown in Figure 4B. Both WT and the double mutant (H139Y, H176Y) show only one set of weakly coupled ^{15}N , which is simulated using a hyperfine tensor **A** of [2.88, 2.88, 1.76] MHz, with $a_{\text{iso}} = 2.50$ MHz. This hyperfine tensor is determined by the simulation of both X-band and Q-band ^{15}N -HYSCORE spectra, as shown in Figure 4C and 4D (Note that both WT and DM show the same HYSCORE spectrum, see Figure 4D). The weak ^{15}N hyperfine interactions are assigned to the remote nitrogens $^{15}\text{N}_{\epsilon}$ of the

equatorial imidazole rings, [35] as they are approximately 4.5% of that of the coordinated nitrogen, which is typical for imidazole-bound paramagnetic spin centers, such as imidazole-bound copper, vanadium and Rieske-type [2Fe-2S] clusters[35-37].

Besides the two sets of ^{15}N hyperfine interactions arising from the $^{15}\text{N}_\delta$ and $^{15}\text{N}_\epsilon$ of equatorially bound histidines, we did not observe other weak hyperfine interactions of ^{15}N as might be expected from a possible axial histidine. This suggests that there is no axial histidine ligand in WT protein. Indeed, we were able to show that the axial ligand is an exchangeable water ligand for both WT and the double mutant, as is evident from ^{17}O ($I = 5/2$) hyperfine interaction ca. 1.82 MHz observed from both ^{17}O HYSORE (Figure 4D) and ENDOR (Figure 4E) experiment on the samples enriched with H_2^{17}O . This ^{17}O hyperfine interaction is consistent with that of an axial water ligand binding a Cu(II) center in the literature[38,39]. The axial water ligand is further confirmed by observing the exchangeable proton by Q-band Davies ENDOR (Figure 4F), which is simulated by using the ^1H hyperfine tensor A [-2.9, -2.8, 6.0] MHz, with the dipolar hyperfine T 2.95 MHz, corresponding to the distance of Cu-H \sim 2.99 Å. [40].

Taken together, these data show that there is no axial histidine binding in either the WT or the double mutant (H139Y, H176Y), and that copper coordination was unchanged by this mutation. This suggests that C-terminal histidines are in fact *not* acting as a fifth, axial ligand, but are instead displacing an equatorially bound N-terminal octarepeat histidine, giving equivalent coordination environments in both WT and DM proteins. We then produced the mutant (H84Y), which only has three octarepeat histidines. This mutant produced equivalent CW spectra to wild type, with

four equatorial histidine ligands, and by NMR produced a slightly stronger *cis* interaction than in wild type, presumably because N-terminal histidines could no longer fully coordinate copper on their own (Figure S4). Combined with NMR evidence that a C-terminal histidine is driving the *cis* interaction, these data suggest that an N-terminal histidine is swapped out for a C-terminal histidine during the protein's *cis* interaction.

Hyperfine Coupling	Origin	Conclusion
a_{iso} : 55 MHz in CW	Coordinated nitrogen on equatorial histidine	
a_{iso} : 2.50 MHz in Mims ENDOR and HYSCORE	Remote nitrogen on equatorial histidine	-
T : 2.95 MHz in Davies ENDOR	Exchangeable proton of axial water	-
A : 1.82 MHz in HYSCORE and Mims ENDOR	Oxygen from H ₂ ¹⁷ O	Presence of axial water
Absence of weak coupling of ¹⁵ N in Mims ENDOR	Axial histidine ligand	No axial histidine

Table 1: Summary of couplings from EPR experiments and their meanings.

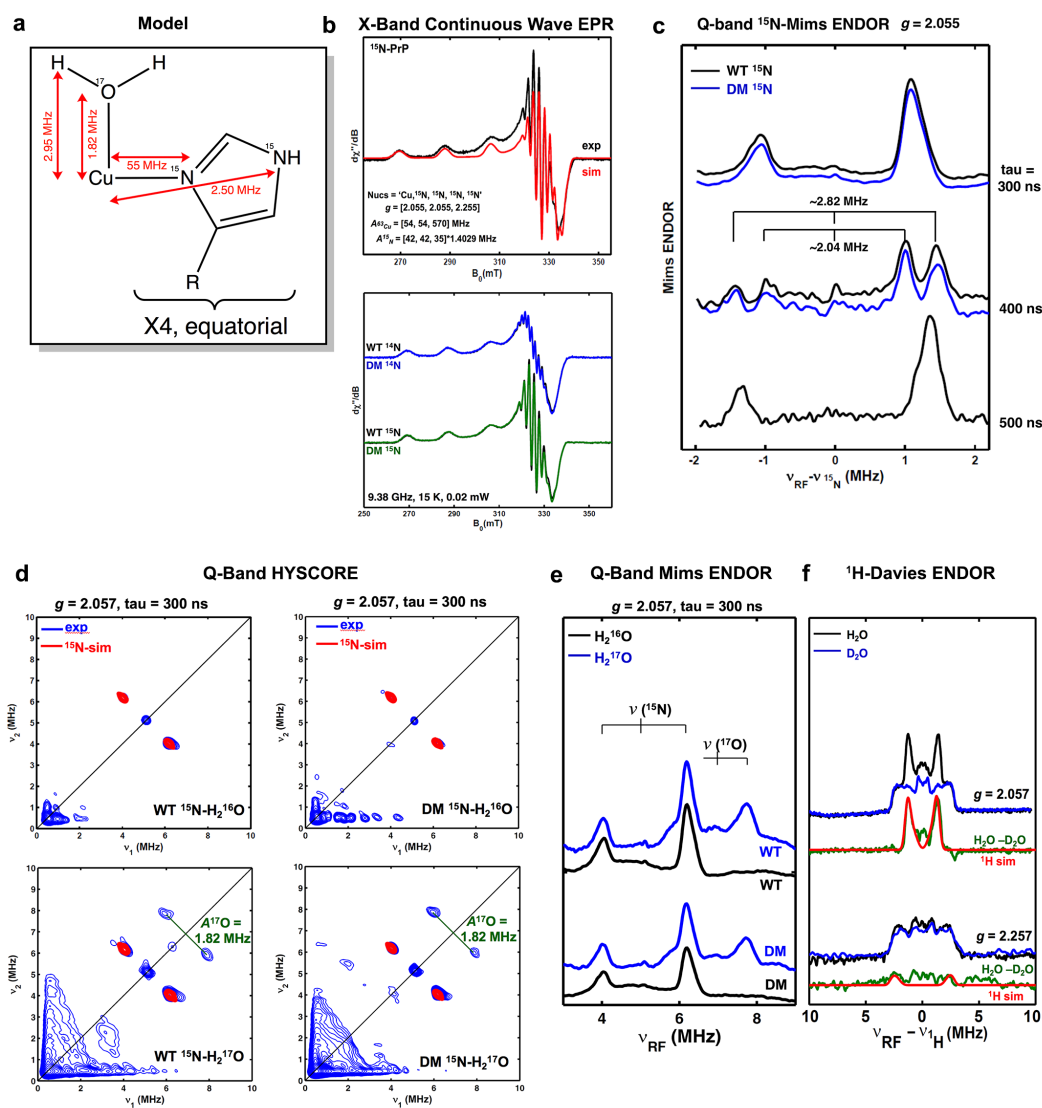


Figure 4: **a)** Representation of the copper site. **b)** X-band continuous wave EPR spectra of WT PrP^C in agreement with simulation based on four equatorial nitrogen ligands and comparison of WT PrP^C to (H139Y, H176Y) PrP^C (labelled DM, for double mutant). **c)** Q-band ^{15}N -Mims ENDOR showing weakly hyperfine interaction for both WT and DM. Varying tau values were used for confirming the Mims-hole effect. **d)** Q-band HYSORE EPR spectra showing weakly coupled remote ^{15}N from histidine and axial ^{17}O from water. **e)** Q-band ^{17}O Mims ENDOR, confirming axial water coordination. **f)** ^1H -Davies ENDOR showing the disappearance of an exchangeable proton from water in when D_2O is used as solvent.

Pathogenic insertion and deletion mutation of histidine-containing octarepeat segments are explained by this model and supported by NMR experiments

An important class of pathogenic mutations in the prion protein involves the insertion of one or more extra copies of the histidine containing octarepeat segment. Mutations leading to extra octarepeats are associated with familial prion disease, and there is a drastic and sudden shift towards early onset disease when there are five or more extra octarepeat insertions[41]. To study these mutations, we employed the same NMR experiments listed above with one equivalent of copper. As shown in Fig. 5, insertion of three extra histidine containing octarepeats did not inhibit the observed *cis* interaction, four extra histidines slightly weakened it, and five extra histidines almost completely inhibited the *cis* interaction. This suggests that insertion mutations sufficient to cause early onset prion disease may act by chelating copper away from C-terminal histidines and preventing the otherwise neuroprotective *cis* interaction. Alternatively, it is possible that the interaction is prevented by an increased entropic penalty due to the longer distance between the termini. In addition to insertional mutations, there are also deletion mutations in this region: deletion of one octarepeat segment does not cause prion disease, but deletion of two segments does[42-44]. This is consistent with the notion that three histidines from the octarepeat and one histidine from the C-terminus are involved in the *cis* interaction.

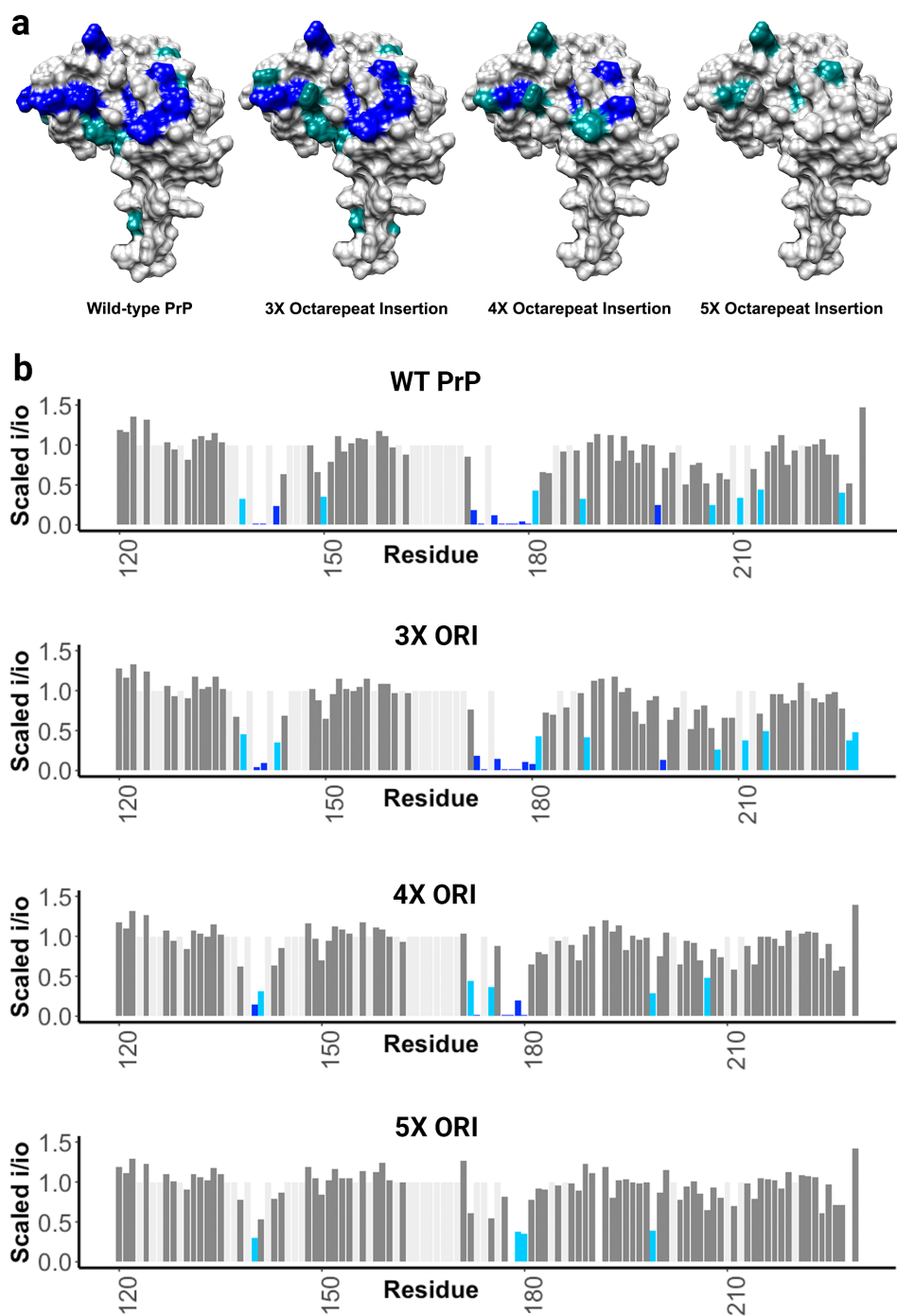


Figure 5: **a)** Surface representations showing areas engaged in the *cis* interaction, as measured by the intensity reduction of NMR cross peaks, plotted on PDB: 1XYX. Five additional octarepeat regions results in a strong decrease in the *cis* interaction. **b)** Bar plots showing the magnitude of the peak intensity reduction derived from the paramagnetic relaxation effect (PRE) on specific residues of the protein's C-terminal domain, with 1 equivalent of CuCl_2 at pH 6.0 in 10 mM MES buffer for all protein samples.

Mutation of C-terminal histidines enhances spontaneous currents

Certain mutations in the central region of PrP, such as $\Delta 105-125$ (referred to as ΔCR) have been observed to cause spontaneous cationic currents in a variety of cell lines and in primary neurons[13]. The currents caused by CR mutations are suppressed by coexpression of wild-type PrP, which mirrors the ability of coexpressed WT PrP to suppress the neurotoxicity of these mutations in transgenic mice[10]. C-terminal antibodies that are neurotoxic when injected into the mouse brain also cause spontaneous currents. We attribute the spontaneous currents and neurotoxicity observed in these scenarios to a weakening of the N-C inter-domain interactions within the PrP molecule[11,21]. We therefore tested whether the H139Y,H176Y mutations, by weakening the cis interaction, caused spontaneous currents in cultured cells.

Using whole-cell patch-clamping of N2a cells held at -90 mV, we observed spontaneous currents for (H139Y,H176Y), and not for a wild-type control (Figure 6). We used a -90 mV holding potential, which is more hyper-polarized than the normal resting potential of N2a cells (-70 mV), to enhance our ability to detect spontaneous currents; we have shown that these currents are voltage-dependent, being greater at more hyper-polarized membrane potential[11]. Consistent with studies of CR PrP mutants, the currents caused by H139Y,H176Y were suppressed by the addition of pentosan polysulfate (PPS), a polymer that sequesters the N-terminal domain of PrP[11].

Pyrenebutyrate (PB) is a polyaromatic, negatively charged small molecule that binds to positively charged groups such as the side chains of arginine and lysine. By

shielding the positive charges, PB facilitates the ability of polybasic peptide regions, like those found at the N-terminus of PrP, to penetrate cell membranes[45-47]. We found (Figure 6b) that the presence of PB greatly enhanced the spontaneous currents caused the Δ 105-125 mutation, even when recorded at -50 mV, a potential at which currents cannot normally be observed[11]. By using PB to enhance the detectability of spontaneous currents, we found that the (H139Y, H176Y) mutation caused currents at -70 mV, the normal resting of N2a cells, whereas no currents were detected at this potential for WT PrP (Figure 6b).

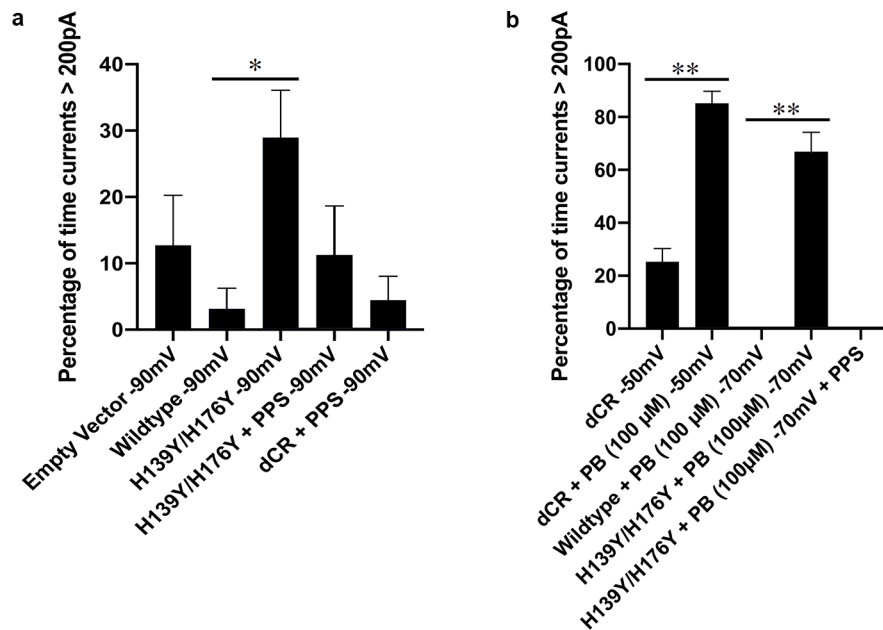


Figure 6: **a)** Comparison of cells transfected with empty vector (N=10), wild-type PrP (N=5), (H139Y,H176Y) PrP (N=20), and Δ CR PrP (N=10) showing that the H139Y,H176Y mutations significantly enhance spontaneous currents at a hyperpolarized holding potential (-90 mV) (* $p=0.045$, $\alpha=0.05$, one tailed two sample t-test), and these currents are suppressed by the addition of pentosan polysulfate (PPS). **b)** Comparison of cells expressing wild-type PrP (N=10), (H139Y,H176Y) PrP (N=10), and Δ CR PrP (N=9) showing that the H139Y,H176Y mutations significantly enhance spontaneous currents at -70 mV in the presence of pyrenebutyrate (** $p<0.00001$), and these currents are suppressed by pentosan polysulfate. The Δ CR mutation enhances currents in the presence of pyrenebutyrate, even at -50 mV (** $p<0.00001$). Error bars show the standard error of the mean.

Protein molecular dynamics (MD) simulations and density functional structure calculations of copper binding in PrP^C

Histidines from both domains appear to be capable of cooperatively coordinating a copper ion, however, the specific His residues involved in this interaction and their location in the Cu²⁺ coordination sphere is not yet known. Starting from an initial coordination state where Cu²⁺ is bound by the four N-terminal His residues in a square planar coordination environment we identified eight additional possible configurations if one of the OR His residues is swapped for either His139 or His176. Using all-atom molecular dynamics simulations, we acquired a total of 675 ns of simulation time over all of the Cu-PrP^C configurations considered. We performed an additional seven simulations where two of the OR His residues are exchanged for His139 and His176 simultaneously (for a total of 285 ns of simulation time). While the specific atoms that comprise the Cu²⁺ coordination environment are different between each simulation, the number of atoms and the type of coordinating atoms immediately surrounding the Cu²⁺ center remain unchanged. We used the Cu²⁺ center and the imidazole heavy atoms (non-H-atoms) of the His residues that are involved in Cu coordination in each simulation along with the protein backbone heavy atoms of helix 2 and helix 3 as a common reference for accessing conformational stability. A clustering analysis was performed (details in methods section). Although there were no explicitly-bound water molecules at the Cu²⁺ axial positions, water molecules tended to occupy these sites for the majority of the simulation time, typically with no exchange or 1-2 waters exchanging during the course of the simulation. A persistent H-bond

interaction was observed in several simulations between the interacting C-terminal Glu residues and one of these axially-retained waters. These results suggest that a His exchange between the N- and C-terminal domains holds the N-terminal OR region close to the C-terminal domain and that additional stabilization is afforded through electrostatic interactions between the cationic copper site and anionic residues in the C-terminus. Importantly, however, we also observe stable close-approach and these same stabilizing electrostatic interactions in the absence of His exchange, with the Cu^{2+} center bound by only the OR regions. This observation confirms that initial close approach of the Cu^{2+} -bound OR region is already a favorable event and that His exchange then occurs as a further stabilizing consequence of the close association. An equilibrated, energy-minimized example of this interaction involving three OR His residues and C-terminal His176 simultaneously coordinating Cu^{2+} is shown in Figure 7.

To further characterize the His exchange event within the Cu^{2+} coordination environment we employed density functional structure calculations to assess the free energy differences between several potential exchange mechanisms. The His residues were modeled as 4-methylimidazole, representing the side chain, with the N_ϵ -position protonated and the N_δ -position available for metal coordination. Axial waters were excluded from the $[\text{Cu}^{2+} (\text{4-methylimidazole})_4]^{2+}$ structure as these are only weakly bound and tend to form H-bonds instead of coordinate covalent interactions. We assessed two potential exchange mechanisms: *i*) an associative route, whereby the Cu^{2+} center coordinates a 5th imidazole moiety in an axial position, which we hypothesize

would then displace an equatorial imidazole in a subsequent step, or ii) a dissociative route where one of the four imidazole moieties is first exchanged for a water molecule and then this water is subsequently exchanged for another imidazole moiety (representing coordination of a C-terminal His residue). Comparing the relative free energies ($\Delta G_{(aq)}$) for the associative vs dissociative route, we find that both are relatively low, at +30.5 and +24.2 kJ/mol, respectively, suggesting that both mechanisms could contribute to ligand exchange. These estimates are from model coordination environments, however, and we anticipate that within the protein, the protein is likely to contribute significantly. While electrostatic interaction tends to draw the Cu^{2+} -bound N-terminal OR region toward the C-terminal domain, the steric bulk of the protein is likely to preclude formation of a crowded 5-His intermediate.

Discussion

Recent evidence shows that the flexible N-terminus of the prion protein acts as a toxic effector, and that this toxicity is down-regulated by interaction with the globular C-terminus[11,14]. Consistent with this model, deletions within the central region linking the two domains, as well as antibodies recognizing the region in the C-terminal domain that docks with the N-terminus, produce toxic effects in cultured neurons and in brain tissue. We hypothesize that these effects are caused by a disruption of the protein's self-regulation, which allows its N-terminus to extend away from the C-terminal domain, allowing aberrant interactions with the plasma membrane or membrane-bound receptors. NMR, EPR, and chemical cross-linking/MS studies

strongly support a physical interaction between the N- and C-terminal domains of PrP[11,15,18,21].

Copper ions have been suggested to play a key role in mediating the interaction between the two domains of PrP, although the molecular details are not fully characterized. It is known that Cu^{2+} binds histidines in the octarepeat region of the protein's N-terminus, and that Cu^{2+} drives the *cis* interaction, but how does Cu^{2+} interact with individual amino acids to carry out this function? In this work, we show that two highly conserved histidines in the C-terminal domain of PrP are essential for the protein's *cis* interaction, and that their substitution with residues that do not bind copper diminishes the interaction, and also induces spontaneous ionic currents associated with an unregulated N-terminal domain. N- and C-terminal histidines work in synchrony to stabilize the *cis* interaction, suggesting that together they co-bind a copper ion, which serves as an inter-domain tether. Because the coordination environment of the copper is unchanged by this event, our data suggest that an N-terminal histidine is swapped with a C-terminal histidine, thereby stabilizing the *cis* interaction. An energy minimized example of this interaction is shown in Figure 7. Whereas previous PrP^C structural models suggested that Cu^{2+} coordination was limited to the protein's N-terminal domain, we find instead that both domains participate in binding the metal ion.

Similar, but rare, intra- and inter-domain copper-sharing mechanisms are observed in other protein systems. In blue copper proteins, copper links two domains, using three ligands from one domain and one ligand from another[48]. The copper

chaperone Atx1 transfers copper to the Ccc2 ATPase through a transient intermediate in which the copper is co-bound by cysteines from both proteins[49]. A similar copper handoff occurs in the CusCBAF export pump in *E.coli*, and is mediated by methionine ligands[50]. Despite the existence of these interdomain and interprotein copper bridges in other protein systems, PrP^C has not previously been known to display these structures. It is established that the N-terminus of PrP^C binds copper[26,27,29,30,51,52], and there is evidence in the literature that the C-terminus can as well[53-56]. However, this work is the first to demonstrate a non-local interaction, with a copper ion bridging N- and C-terminal histidine ligands and thereby stabilizing an inter-domain interaction. In this model, the affinity of Cu²⁺ for histidine residues in the N-terminal octarepeat region ($K_d=0.1$ nM), although high, is nevertheless weak enough to allow for exchange with histidine residues in the C-terminus.

The details of the *cis* interaction observed here provide a new explanation for a specific set of genetic prion diseases involving octarepeat variations. Individuals with at least five extra inserts of the octarepeat segment (nine total repeats) develop early onset prion disease. Based on the exceptionally high binding affinity between copper and this expanded OR segment ($K_d < 0.01$ nM), early onset disease was previously hypothesized to be due to either a loss of a copper dependent function of PrP^C, or a loss of copper mediated protection against misfolding[41]. In light of the new findings presented here, we suggest an alternative interpretation: the toxicity of these mutations may be due to the extra octarepeat histidines chelating copper away from C-terminal

histidines, thereby disrupting the regulatory *cis* interaction. In addition, deletion of one octarepeat segment is nontoxic in humans, but deletion of two or more results in prion disease[42-44]. This is consistent with the notion that three histidines from the octarepeat and one histidine from the C-terminus are necessary for the *cis* interaction. Lastly, specific C-terminal point mutations that reduce negative charge and increase positive charge, such as D177N and E199K in mice (D178N and E200K in humans), are located close to H176, and therefore likely to reduce or prevent C-terminal copper binding, which would also impair the *cis* interaction.

The experiments described in this study have utilized a 1:1 Cu^{2+} : PrP^C stoichiometry. This stoichiometry is probably physiologically relevant, given the subnanomolar affinity of PrP^C for Cu^{2+} and the Cu^{2+} concentrations thought to be present at the synapse. However, we have shown previously that coordination of Cu^{2+} by PrP^C changes with concentration[29]. Studies into the nature of this interaction as a function of Cu^{2+} concentration may provide further insight into the *cis* interaction, PrP^C function and familial disease. Additionally, future investigations will consider zinc, another metal known to bind to PrP^C.

In summary, we have shown that two histidine residues in the C-terminal domain of PrP^C drive a protective *cis* interaction between the N- and C-terminal domains. We have designed a novel mutation, involving simultaneous deletion of these two histidines, that impairs N-C interaction and enhances spontaneous currents associated with neurotoxicity. Thus, our work furthers the body of evidence for a neuroprotective *cis* interaction in the protein. These findings suggest a novel PrP^C-

mediated neurodegenerative mechanism whereby toxic prion oligomers, antibodies, and mutations elicit their effects through disruption of this interaction. Therefore, small molecule drugs or antibodies that stabilize and reinforce the *cis* interaction are potential therapeutic avenues to protect against toxicity in prion disease.

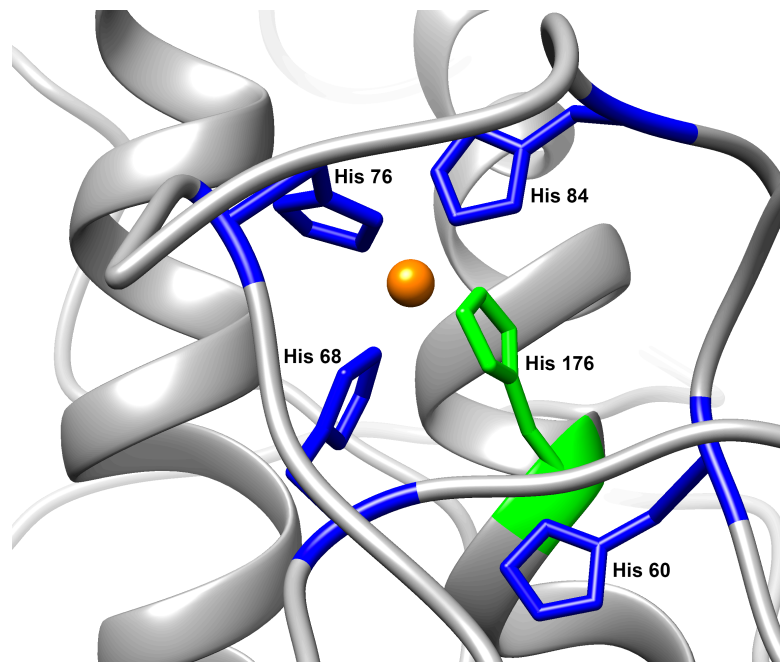


Figure 7: A structural explanation for the results of this paper. An N-terminal histidine (blue) swaps out for C-terminal His176 histidine (green) during the protein's *cis* interaction, creating a copper tether between the two domains.

Materials and Methods

¹⁵N Labeled Protein Expression

Starting with the full length wild-type mouse prion protein in the pJ414 vector backbone (DNA 2.0), we used QuickChange site-directed mutagenesis PCR to construct mutants, with primers generated manually and by www.primerdesigner.com. DNA was transformed into *E. coli* BL21Star (DE3) cells (Invitrogen) and expressed in M9 minimal media supplemented with 1 g/L ¹⁵N ammonium chloride (Cambridge Isotope Labs). Cells were grown at 37 °C until they reached an OD600 of 1.0, at which point the temperature was dropped to 30 °C and protein expression induced with 1 mM isopropyl-1-thio-D-galactopyranoside (IPTG). Cells were allowed to express for 20 hours. Inclusion bodies were washed, then treated with 8 M guanidine HCl in pH 8 tris-acetate buffer to extract proteins. The extracted proteins were purified by immobilized metal affinity chromatography, allowed to fold overnight at pH 8, then transferred into pH 4.5 sodium acetate buffer by size exclusion chromatography. The proteins were then dialyzed into Milli-Q ultrapure water and purified further by reverse phase HPLC using C4 silica resin. Identity and purity were checked using a Sciex X500b mass spectrometer. The proteins were lyophilized, and quantified by UV-Vis spectrophotometry before use.

Construct	<i>Cis</i> Interaction
Wild-type Mouse PrP ^C	<i>Cis</i> Interaction, four his ligands
H139Y	Interaction shifted towards H176
H176Y	Interaction shifted towards H139
H186Y	Interaction maintained
H186R	Interaction maintained
H139Y,H176Y	Strongly reduced interaction
H139N,H176N	Strongly reduced interaction
H139A,H176A	Strongly reduced interaction
M139A,I138A,F140A	Misfold / no data on interaction
N172A,N173A,V175A,V179A,N180A	Interaction maintained
Segment 90-230	No interaction
H176N,N172H	Interaction moved down helix
H176N,N180H	Interaction moved up helix
3XORI	Very weakly reduced interaction
4XORI	Weakly reduced interaction
5XORI	Strongly reduced interaction
H84Y	Slightly stronger <i>cis</i> interaction than WT
H95Y, H110Y	No difference in <i>cis</i> interaction from WT

Table 2: Constructs tested by NMR in this paper

Nuclear Magnetic Resonance Spectroscopy

All samples were made to pH 6.0 in 10mM 2-(*N*-morpholino)ethanesulfonic acid (MES) buffer (Sigma), using potassium as a counterion and containing 10% D₂O. For all samples, the protein was added to a concentration of 300 μM. For samples with copper, CuCl₂ was used at 300 μM. ¹H-¹⁵N HSQC spectra were recorded at 37 °C on a Varian INOVA 600 MHz spectrometer (Varian, Santa Clara, CA) at UCSC NMR facility (Santa Cruz, CA), and on a Bruker 800 MHz spectrometer also at UCSC. NMR spectra were analyzed with NMR Pipe and Sparky using assignments transferred from previous experiments by visual inspection, and figures were made using Chimera and R. To determine a cutoff i/i_0 value to separate the residues involved in the *cis* interaction from the rest of the protein, we performed a kernel density estimation on the data using

a Gaussian smoothing kernel. To eliminate the effects of differential unspecific peak intensity reduction across mutants, the data were scaled so that the center values of each mutant's group of unaffected peaks were aligned. We divided the residues into three categories based on their i/i_0 values: strongly affected (dark blue), weakly affected (light blue) and unaffected (grey). These divisions were created by using the local minimum separating the affected from unaffected residues in the wild-type protein ($i/i_0 = 0.35$), and dividing the affected peaks into two groups ($i/i_0 = 0$ to 0.175 , and $i/i_0 = 0.175$ to 0.35).

Electron Paramagnetic Resonance Spectroscopy

The X-band (9.38 GHz) continuous-wave (CW) EPR spectra were recorded on a Bruker (Billerica, MA) EleXsys E500 spectrometer equipped with a super-high Q resonator (ER4122SHQE). Cryogenic temperatures were achieved and controlled using an ESR900 liquid helium cryostat in conjunction with a temperature controller (Oxford Instruments ITC503) and gas flow controller. CW EPR data were collected under slow-passage, non-saturating conditions. The spectrometer settings were as follows: temperature = 15 K, conversion time = 40 ms, modulation amplitude = 0.8 mT, and modulation frequency = 100 kHz; other settings are given in corresponding figure captions. Simulations of the CW spectra and the following pulsed EPR spectra were performed using EasySpin 5.1.10 toolbox[57,58] within the Matlab 2014a software suite (The Mathworks Inc., Natick, MA).

Q-band (~34.0 GHz) pulse ENDOR experiments were performed on a Bruker Biospin EleXsys 580 spectrometer equipped with a 10 W amplifier and a R.A. Isaacson cylindrical TE₀₁₁ resonator in an Oxford CF935 cryostat. ENDOR measurements were performed at 20 K by employing the Mims pulse sequence ($\pi/2$ - τ - $\pi/2$ -RF- $\pi/2$ - τ -echo) for small hyperfine couplings[59] or Davies pulse sequence (π -RF- $\pi/2$ - τ - π - τ -echo) for larger hyperfine couplings[60]. ENDOR spectra were collected stochastically by randomly hopping the RF excitation frequency[61]. Pulse sequences were programmed with the PulseSPEL programmer via the Xepr interface.

For Mims-ENDOR experiments, [59] the ENDOR intensities are modulated by the response factor (R) which is a function of the hyperfine coupling A and the time interval (τ) between the first and the second $\pi/2$ microwave pulse in the three-pulse sequence: $R \sim [1 - \cos(2\pi A\tau)]$. When $A\tau = n$ ($n = 0, 1, 2, 3 \dots$), this factor will be zero, corresponding to a minima in the ENDOR response, i.e., the hyperfine “suppression holes” in Mims-ENDOR spectra. This Mims-hole effect can be avoided by adjusting the τ value, as shown in Figure 4B.

X-band and Q-band HYSORE spectra were recorded on the Bruker Biospin EleXsys 580 spectrometer with a split-ring (MS5) resonator at 20 K using the pulse sequence $\pi/2$ - τ - $\pi/2$ - t_1 - π - t_2 - $\pi/2$ - τ -echo. The pulse length for inversion pulse (t_π) and the $\pi/2$ pulse ($t_{\pi/2}$) was 32 ns and 16 ns, respectively. Eight-step phase cycling was used. Time-domain spectra were baseline-corrected (third-order polynomial), apodized with a hamming window, zero-filled to eight-fold points, and fast Fourier-transformed to yield the frequency-domain spectra.

Whole-Cell Patch Clamp Experiments

Recordings were made from N2a cells 24–48 hr. after transfection. Transfected cells were recognized by green fluorescence resulting from co-transfection with pEGFP-N1. Whole-cell patch clamp recordings were collected using standard techniques. Pipettes were pulled from borosilicate glass and polished to an open resistance of 2–5 megaohms. Experiments were conducted at room temperature with the following solutions: internal, 140 mM Cs-glucuronate, 5 mM CsCl, 4 mM MgATP, 1 mM Na₂GTP, 10 mM EGTA, and 10 mM HEPES (pH 7.4 with CsOH); external, 150 mM NaCl, 4 mM KCl, 2 mM CaCl₂, 2 mM MgCl₂, 10 mM glucose, and 10 mM HEPES (pH 7.4 with NaOH). Current signals were collected from a Multiclamp 700B amplifier (Molecular Devices, Sunnyvale, CA), digitized with a Digidata 1440 interface (Molecular Devices), and saved to disc for analysis with PClamp 10 software.

Molecular dynamics simulations

The model of the Cu²⁺-bound mouse PrP^C protein was constructed from a representative structure from the NMR-derived dataset for 1XYX[62] (mouse PrP^C fragment 121-231). Residues 23-120 were added, with the ϕ and ψ angles for residues 57-91, the OR region, were taken from Pushie and Vogel[63]. Both Cys residues were maintained in a disulfide cross linkage, and all His side chains were singly protonated at the N δ ring position, leaving N ϵ available to potentially serve as a donor atom for copper. An initial simulation maintained Cu²⁺ coordination to each of the 4 OR His residues (N ϵ bound), in a square planar geometry, parameterized based on extended X-

ray absorption fine structure (EXAFS) spectroscopy and DFT calculations[63,64]. MD simulations were performed with GROMACS 2016.3[65] using the OPLS-AA force field[66] modified to include parameterization of the square planar Cu^{2+} center[63]. The initial structure was subjected to steepest-descent energy minimization in the presence of explicit solvent, using 32360 TIP4P waters, without constraints. The starting Cu-MoPrP^C (23-231) structure was simulated for 100 ns to allow the N-terminal region to equilibrate. While the N-terminal domain remained disordered it was observed to collapse and remain relatively compact. During this initial equilibration the N-terminally-bound Cu^{2+} site was observed to approach the face of the C-terminal domain identified in experiments (*vide infra*), similar to the interactions described previously in Evans et al. [18]. At the end of the equilibration phase the Cu^{2+} site was modified to allow each of the OR His residues to exchange with either H139 or H176. After the coordinating His parameters were swapped the steepest descent minimization was re-run to obtain a new starting structure for each of the His-exchanged models. Trajectories in the simulations were recalculated every 2 fs and structures were saved every 10 ps. Each simulation, including a simulation where no C-terminal exchange was performed (only coordination by the OR His residues), was run for 80 ns with an NPT ensemble, at 300 K and 1 atm, with each preceded by a 5 ns equilibration phase which was not included in analysis.

Conformational stability of the interacting Cu^{2+} -binding environment and the C-terminal domain of the protein was analyzed by grouping the Cu^{2+} center and the heavy atoms from each coordinating His imidazole ring with the backbone heavy atoms

from Helix 2 and Helix 3. This allowed each of the exchange models to be compared using the same number and type of atoms: Helix 2, Helix 3, and Cu(imidazole)₄. The RMSD of these atoms were used in cluster analysis (with a 0.045 nm cutoff using *gmx cluster*) to quantify the variability in conformational stability. We hypothesize that if a given Cu/His configuration has a low number of clusters and if the dominant cluster represents a stable close association between the OR region and the C-terminal domain then these were likely to be more favorable configurations of the system as opposed to configurations that gave rise to broad ranges of low-population conformational states. We found that all of the configurations with clusters that represented more than 50% of the sampled structures during the simulation also had stabilizing electrostatic interactions between the Cu²⁺ coordination environment and anionic residues in the C-terminal domain. Importantly, of all the configurations that included two His exchanges only the simulation where His61 and His69 (the first two OR His residues) were swapped for His176 and His139 respectively resulted in a stable conformation, all other two-His exchange configurations resulted in disordered interactions between the Cu²⁺ coordination environment and the C-terminal domain. Of the single His exchange simulations those that involved exchange of the first or last OR His residue (His61 or His85) tended to be dominated by a single stable conformation that represented 80% or more of the sampled conformations, while the simulation with the 4th OR His exchanged for His176 had two dominant and closely-related conformations that represented 72% of all structures sampled. Close inspection of the dominant clusters

revealed that most simulations formed stabilizing electrostatic interactions between the Cu^{2+} coordination site and Glu207 and Glu211 in the C-terminal domain.

Density functional structure calculations

Density functional calculations employed Gaussian 16, revision A.03[67], with the B3LYP functional method[68] employing the 6-311+G(d,p) basis set on all atoms, and included the Grimme-D3 dispersion correction[69] for geometry optimizations and subsequent harmonic frequency calculations. The long-range stabilizing influence of solvation was calculated from the gas-phase optimized geometries using a self-consistent reaction field dielectric continuum (IEFPCM) [70] with $\epsilon = 78.36$ (for water) and employing the united atom topological model radii (UAHF). Relative free energies between calculated structures followed previously-published methods[64].

Acknowledgements

We thank NIH grants R01GM065790, R35GM131781 (GLM), R35GM126961 (RDB) and R01NS065244 (DAH) for financial support, and NIH instrumentation grant S10OD018455 for acquisition of the 800 MHz NMR spectrometer and S10OD024980 for acquisition of the pulsed EPR spectrometer. This research was enabled in part by support provided by WestGrid (www.westgrid.ca) and Compute Canada Calcul Canada (www.computecanada.ca).

Supporting Information

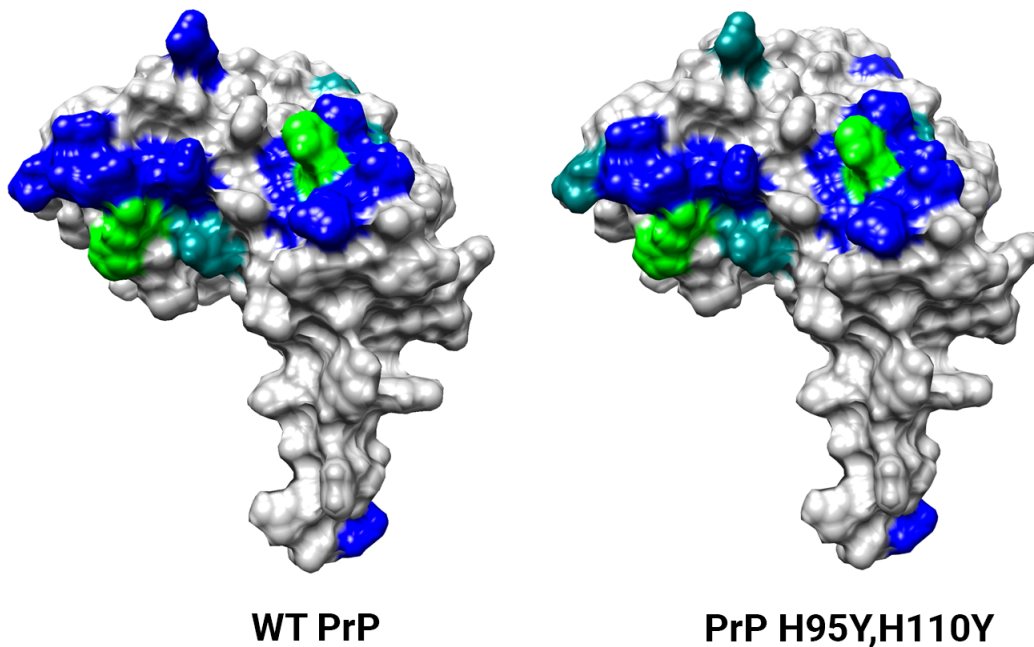


Figure S1. A comparison of peak intensity reduction in WT PrP^C vs. PrP^C (H95Y,H110Y) shows that histidines 95 and 110 are not driving the interaction between the protein's N and C termini, ruling out the possibility that the C-terminus of PrP^C is interacting with copper bound solely to a (H95,H110) complex. Samples were recorded with 300 μ M protein, 10 mM MES buffer pH 6.0, 10% D₂O, at 37 °C, both with and without 300 μ M CuCl₂. Residues that broadened strongly in the presence of copper (dark blue), broadened weakly in the presence of copper (light blue) and histidines (green) are colored. Coordinates for the C-terminal PrP^C structure are from PDB:1XYX.

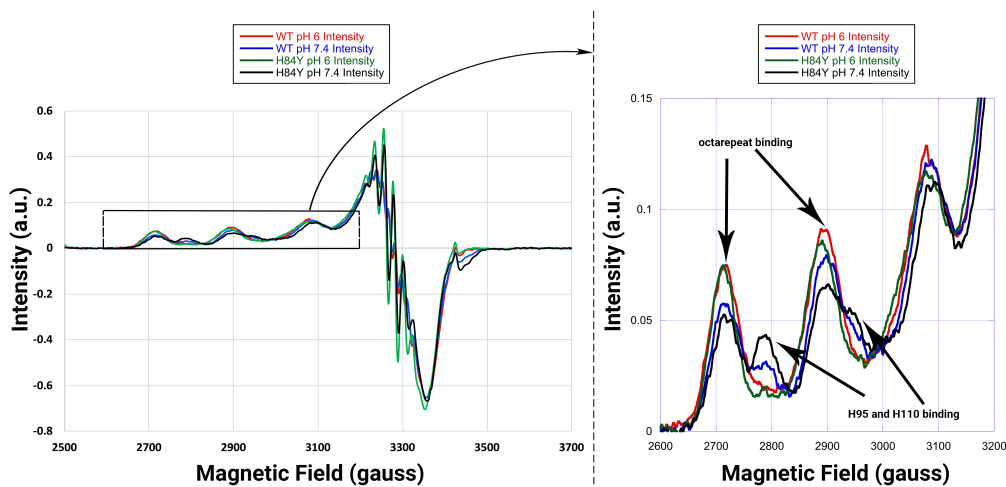


Figure S2. Continuous wave EPR of WT PrP^C and PrP^C H84Y shows that the copper binding to a central region histidine complex (H95,H110) that is observed at pH 7.4 is not observed at pH 6.0. Samples were recorded with 100 μ M PrP, 50 mM MES (pH 6.0) or MOPS (pH 7.4) buffer, 25% glycerol, and 100 μ M CuCl₂. Noise reduction was applied post sample collection. The 4-histidine splitting has an a-parallel of 185 G and a g-parallel of 2.249. The two histidine splitting (H95,H110) has an a-parallel of 159 G and a g-parallel of 2.226.

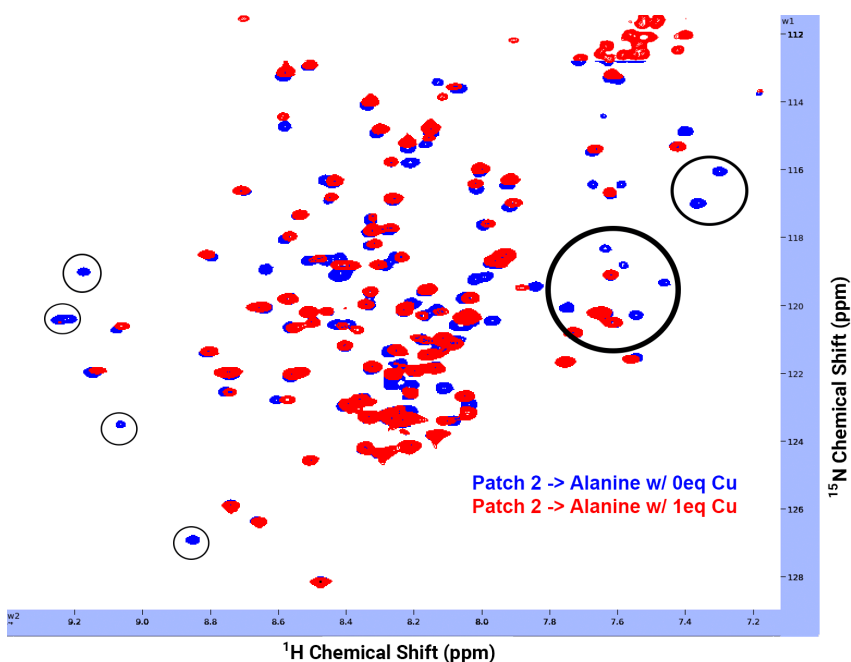


Figure S3. PrP^C (172A,173A,175A,179A,180A) with and without copper shows that residues near His176 do not play a role in the *cis* interaction, highlighting the importance of His176. Samples were recorded with 300 μ M protein, 10 mM MES buffer pH 6.0, 10% D₂O, at 37 °C, both with and without 300 μ M CuCl₂. Because most of the strongly broadened peaks in the protein have been changed in this mutant, we do not have assignments for them. However, we know that they are the peaks that are new to this mutant (inside the big circle). These peaks disappear with copper, indicating that the *cis* interaction is still occurring in this mutant.

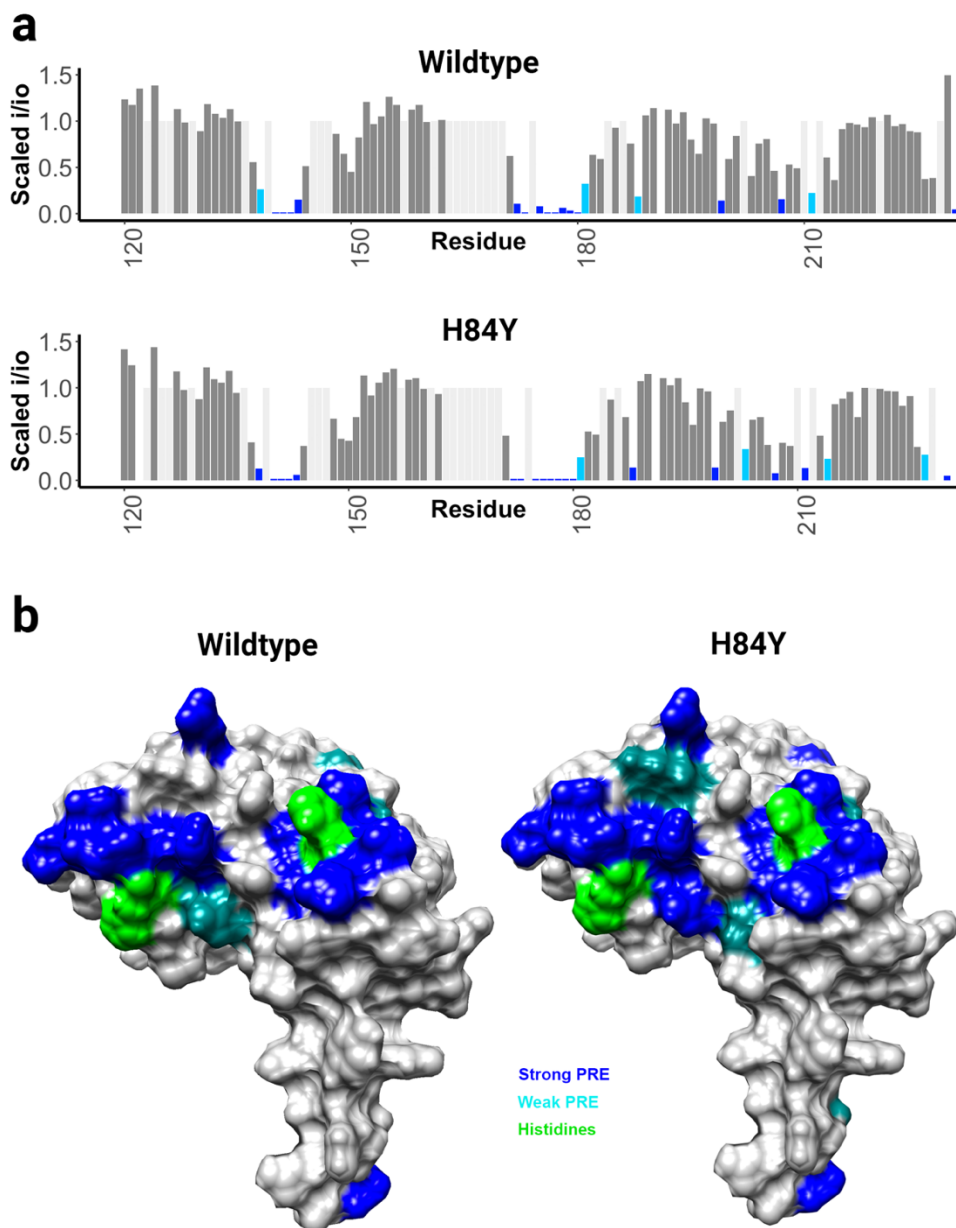


Figure S4. A comparison of peak intensity reduction in WT PrP^C vs. PrP^C H84Y shows that the *cis* interaction is preserved and even strengthened when one octarepeat histidine is deleted. This agrees with the hypothesis that only three out the four octarepeat histidines are involved in the *cis* interaction at any given time. Samples were recorded with 300 μ M protein, 10 mM MES buffer pH 6.0, 10% D₂O, at 37 °C, both with and without 300 μ M CuCl₂. a) Bar plots showing the magnitude of the peak intensity reduction with the addition of one equivalent of copper. b) Surface representations showing broadened areas engaged in the *cis* interaction, as measured by peak intensity reduction. Residues that broadened strongly in the presence of copper (dark blue), broadened weakly in the presence of copper (light blue) and histidines (green) are colored. Coordinates for the C-terminal PrP^C structure are from PDB:1XYX

Chapter 3

Production of Artificially Doubly Glycosylated, ¹⁵N Labelled Prion Protein for NMR Studies Using a pH-Scanning Volatile Buffer System

Kevin M. Schilling, Natalia C. Ubilla-Rodriguez, Conner W. Wells, Glenn L.

Millhauser*

Department of Chemistry and Biochemistry, University of California, Santa Cruz,

CA, 95064 *glenm@ucsc.edu

Introduction and Results

PrP^C contains two N-linked glycosylation sites proximal to the location of many of its pathological mutations[71]. We wished to investigate the effect that these glycans have on the structure of the protein, using nuclear magnetic resonance (NMR). However, uniformly ¹⁵N labelled protein produced for NMR by recombinant expression in *E.coli* does not contain glycans, and other methods such as mammalian or insect expression are neither easily ¹⁵N labelled, nor glycosylated homogeneously, making NMR investigations difficult. Hornemann *et al.* have previously shown that the structure of glycosylated bovine PrP extracted from healthy calf brains is essentially identical to that of unglycosylated recombinant PrP using circular dichroism and one-dimensional ¹H-NMR spectroscopy, but were unable to perform two dimensional NMR due to low protein concentration and lack of isotopic labelling[72].

Recently, advances in bio-orthogonal organic chemistry, coupled with the ability to incorporate unnatural amino acids in expressed proteins, have led to the ability to attach small molecules selectively to specific positions in proteins. Methods to prepare and attach artificial glycans have been published, but these methods have not to our knowledge been applied to ¹⁵N labelled expressed protein, or to create multiple homogenous glycans per protein[73,74].

We initially attempted the procedure from the Schultz laboratory that couples aminoxy sugars onto the ketone of *p*-acetyl-phenylalanine and extends them into longer glycans using glycosyltransferases[73], but we encountered conflicting pH requirements between the reactants. Recombinant prion protein is soluble at low-

medium pH, and the ketone to aminoxy coupling works best at low pH, thus achieving the first synthetic step. However, the glycosyltransferases have published activities near physiological pH. Thus, when the glycan extension reactions were performed in buffer systems typically used for enzymatic ligation, the prion protein precipitated, and when performed in the low salt, low pH buffers that are compatible with the prion protein, the glycosyltransferases were not active. We attempted the reactions at a few select intermediate pH values but were not able to identify solution conditions. We determined that if there *was* an intermediate pH where the prion protein was soluble and the enzymes were active, that the best way to find this, without an exhaustive and reagent-consuming test of many pH values, was to attempt the reaction at all pH values with the reasonable pH range, in one shot. If the reaction buffer could slowly change in pH over time, the reaction would then proceed when both the substrate solubility and enzyme activity pH needs are met.

Carbon dioxide reduces the pH of aqueous solutions through the transient formation of carbonic acid, which dissociates to H^+ and bicarbonate anion. We reasoned, therefore, that an acidified solution prepared with a bicarbonate buffer would slowly drift up in pH due to transfer of protons to bicarbonate base, followed by loss of carbon dioxide. We prepared a mixture of ammonium bicarbonate and acetic acid at pH 6.5. All ions in this mixture are compatible with analysis by mass spectrometry. As carbon dioxide evolves out of solution, the pH rises until an equilibrium is reached among the remaining weak bases (Figures 1,2). The starting and ending pH are determined by the concentration of buffer components, and the rate of pH increase is

affected by stir rate and atmospheric pressure (Figures S7,S8). By varying stir rate and pressure, the duration of pH scanning can be controlled from three hours to indefinitely. Tightly capping the reaction with limited headspace slows down pH drift, and application of a vacuum quickens pH drift. For proteins sensitive to oxygen exposure, this process can be done under an inert atmosphere. We performed both of the enzymatic coupling steps in this buffer. Termination of the reactions was indicated by protein precipitate. Lowering the pH of this solution solubilized the products and analysis by mass spectrometry revealed homogeneously glycosylated protein.

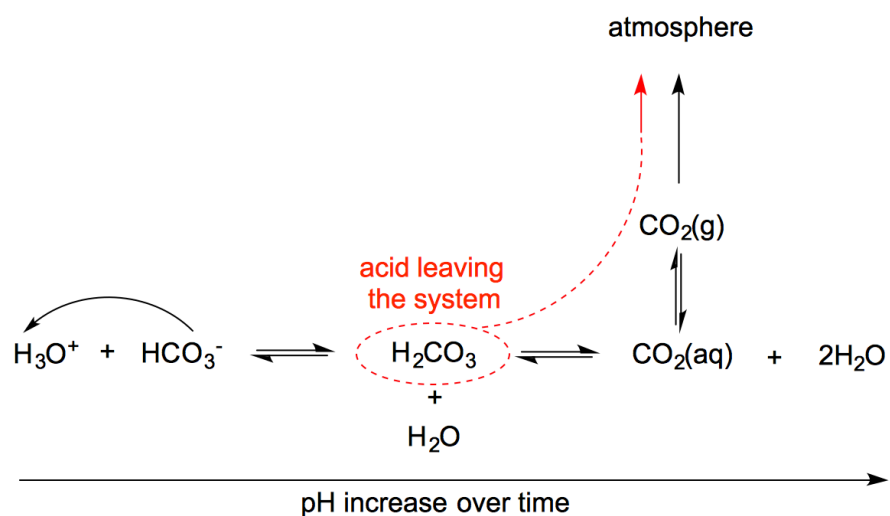


Figure 1: Carbonic acid leaves the system as carbon dioxide, raising the pH of the solution.

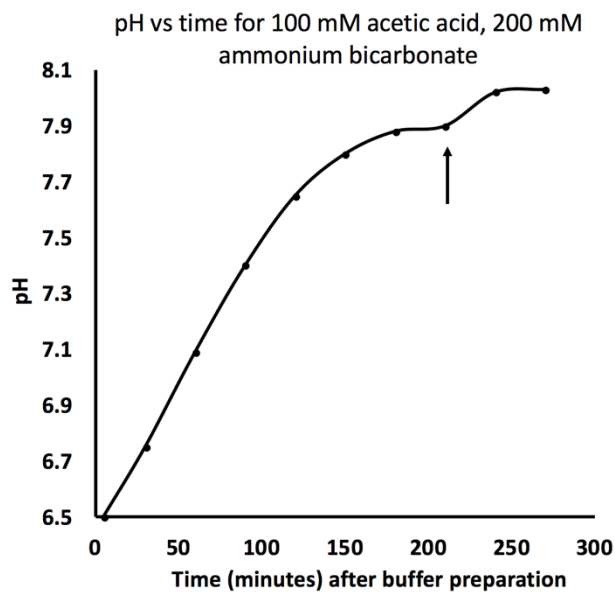


Figure 2: Change in pH over time of 100 mM acetic acid, 200 mM ammonium bicarbonate, with vigorous stirring. Other concentrations that scan over different pH ranges at different rates are presented in the supporting information (Figures S7,S8). The increase in slope at 210 minutes (arrow) is from application of a vacuum to the sample cell.

The synthetic scheme for the glycosylated PrP is shown in Figure 3. Although lower in molecular weight than typical branched PrP^C glycans, we sought to retain fundamental chemical features by terminating with a sialic acid, typical of PrP^C and other proteins of the central nervous system. The sialylation status of PrP^C controls its ability to form toxic misfolded aggregates in *in vitro* protein misfolding cyclic amplification (PMCA) assays, alters the infectivity of these aggregates, and controls the species barrier for transmission of prion disease[75-78].

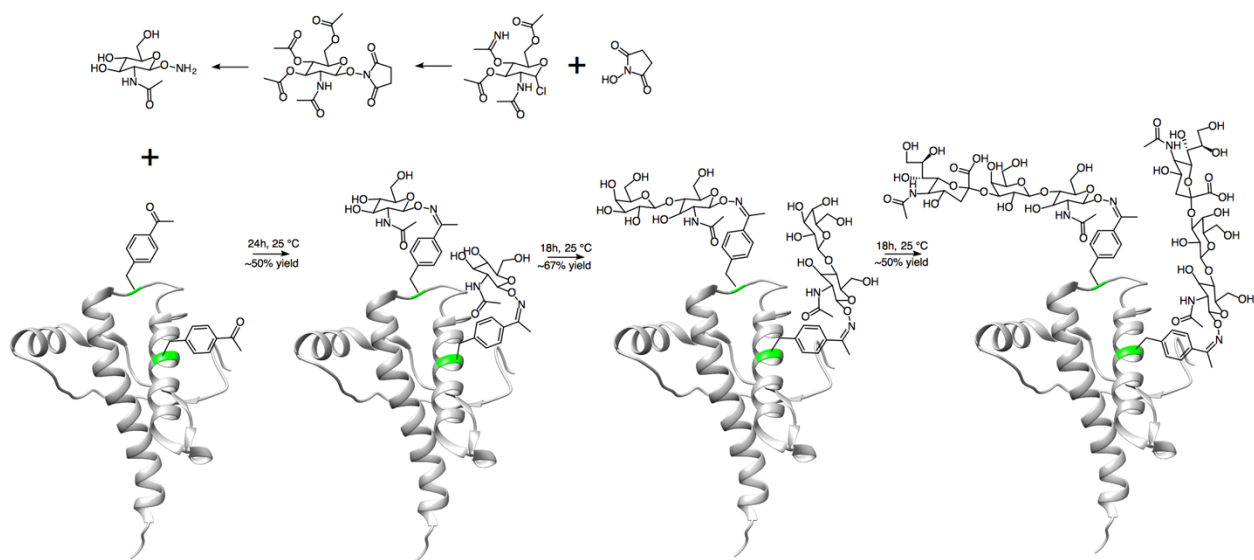


Figure 3: Synthesis scheme for glycosylated PrP. The base structure for this image is PDB: 1XYX, which is an NMR structure of the C-terminus of mouse PrP^C[62].

After successful preparation of the artificially glycosylated prion protein, we performed ^1H - ^{15}N HSQC NMR and circular dichroism spectroscopy to look for any structural effects that the glycans may have on the protein. The NMR spectrum overlapped closely with non-glycosylated prion protein, with the exception of amino acids in close proximity to the glycans, and the circular dichroism spectra overlapped closely with each other as well as with literature spectra[79], indicating that the glycans had not misfolded the protein. (Supporting Information, Figures S5, S6).

In conclusion, we report the artificial glycosylation of ^{15}N labelled prion protein for NMR studies, adding two homogenous trisaccharides at the protein's glycosylation sites, and the verification by NMR and CD that these glycans did not disturb the overall fold of the protein. The required reactions were made possible by a buffer that scans over a pH range, allowing the reactions to proceed when a pH is reached that balances

substrate protein solubility with enzyme activity. In addition, this buffer is volatile, allowing direct use of mass spectrometry during the reactions, without the need for liquid chromatography.

Materials and Methods

To prepare murine PrP with *p*-acetyl-phenylalanine at its two glycosylation sites, we mutated the corresponding amino acid codons (N180 and N196) to the amber stop codon TAG using site-directed mutagenesis PCR. The resulting sequence was murine Met-PrP(23-230, Asn180pAcPhe, Asn196pAcPhe). The *E.coli* strain B-95.AAAfabR, which has many of its TAG codons replaced[80], was co-transformed with this plasmid and with the pEVOL-pAcF plasmid from the Schultz lab, which codes for the aminoacyl-tRNA synthetase (aaRS) and transfer ribonucleic acid (tRNA) corresponding to *p*-acetyl-phenylalanine[81]. The protein was expressed in 1.0 L of M9 minimal media made with 1.0 g ¹⁵N NH₄Cl and 400 mg *p*-acetyl-phenylalanine. The protein was incubated at 37 °C with shaking. At an OD600 of 0.2, arabinose was added to 1.0 mM in order to induce expression of the aaRS and tRNA, and at an OD600 of 0.8, isopropyl-β-D-thiogalactoside (IPTG) was added to 1.0 mM in order to induce expression of PrP, and the culture was incubated overnight at 25 °C. The cells were pelleted and lysed, and inclusion bodies were washed with 1M urea before being extracted with 8 M guanidine hydrochloride and purified by nickel immobilized metal ion chromatography. The protein was brought to pH 8.0 for one day to allow its disulfide bonds to form, then further purified by HPLC on C4 resin, using

water and acetonitrile with 0.1% trifluoroacetic acid, yielding 6 mg. The protein mass was checked by mass spectrometry (23516 g/mol measured, 23519 g/mol expected), and lyophilized and stored at -80 °C (Figure S1). The Advion Expression-L used has mass inaccuracy up to 0.2%.

To prepare the aminoxy N-Acetylglucosamine, the procedure outlined by Liu, *et al.* was followed, which itself references the more detailed protocol in Cao *et al.*[73,82]. (Figure 3). We found the purity of the 2-acetamido-2-deoxy- α -D-glucopyranosylchloride 3,4,6-triacetate to be highly vendor and batch dependent, and had success with material from Combi-Blocks, which was received as a white powder.

To couple the sugar to the mutant PrP, 6 mg of the PrP was dissolved in 200 mM acetic acid, 100 mM ammonium bicarbonate, pH 4.5, and 10 mg aminoxy-N-acetylglucosamine. The reaction was left overnight, and the protein was purified by HPLC on C4 resin, using water and acetonitrile with 0.1% trifluoroacetic acid, yielding 3 mg. The protein mass was checked by mass spectrometry (23937 g/mol measured, 23957 g/mol expected), and lyophilized (Figure S2).

To extend the two single sugars into two disaccharides, 3 mg of the mutant PrP was dissolved in 100 mM acetic acid, 200 mM ammonium bicarbonate, pH 6.5, with 5 mg UDP- α -D-galactose, 5 μ g beta-1,4-galactosyltransferase (R&D Systems 3609-GT-010), and 1 U alkaline phosphatase (Sigma Aldrich 10713023001). The reaction was left overnight, and found to be at pH 7.9 the next day, with the PrP having precipitated. The PrP was resuspended with the addition of glacial acetic acid, and purified by HPLC on C4 resin, using water and acetonitrile with 0.1% trifluoroacetic acid, yielding 2 mg.

The protein mass was checked by mass spectrometry (24257 g/mol measured, 24281 g/mol expected), and lyophilized (Figure S3).

To extend the two disaccharides into two trisaccharides, 2 mg of the mutant PrP was dissolved in 100 mM acetic acid, 200 mM ammonium bicarbonate, pH 6.5, with 2.5 mg cytidine-5'-monophospho-N-acetylneuraminic acid (CMP-Sialic acid), 0.5 U α -2,3-sialyltransferase (Sigma Aldrich S1951-1UN), and 1 U alkaline phosphatase. The reaction was left overnight, and found to be at pH 7.9 the next day, with the PrP having precipitated. The PrP was resuspended with the addition of glacial acetic acid, and purified by HPLC on C4 resin, using water and acetonitrile with 0.1% trifluoroacetic acid, yielding 1 mg. The protein mass was checked by mass spectrometry (24868 g/mol measured, 24863 g/mol expected), and lyophilized (Figure S4).

^1H - ^{15}N HSQC NMR samples were made to pH 6.0 in 10mM 2-(*N*-morpholino)ethanesulfonic acid (MES) buffer, using potassium as a counterion and containing 10% D₂O. For all samples, the protein was added to a concentration of 100 μM . Spectra were recorded at 37 °C on a Bruker 800 MHz spectrometer at UCSC NMR facility (Santa Cruz, CA). NMR spectra were analyzed with NMR Pipe and Sparky using assignments transferred from previous experiments by visual inspection. Circular dichroism spectroscopy was performed on a Jasco J-1500, and the data were analyzed on the CAPITO web server[83].

Acknowledgements

We thank NIH grant R35GM131781 for financial support, and NIH instrumentation grants S10OD016246 and S10OD018455 for acquisition of the circular dichroism spectrometer and 800 MHz NMR spectrometer, respectively. We also thank Drs. K. Sakamoto and S. Yokoyama at the RIKEN Yokohama branch for providing the B-95.AAAfabR *E.coli* strain.

Supporting Information

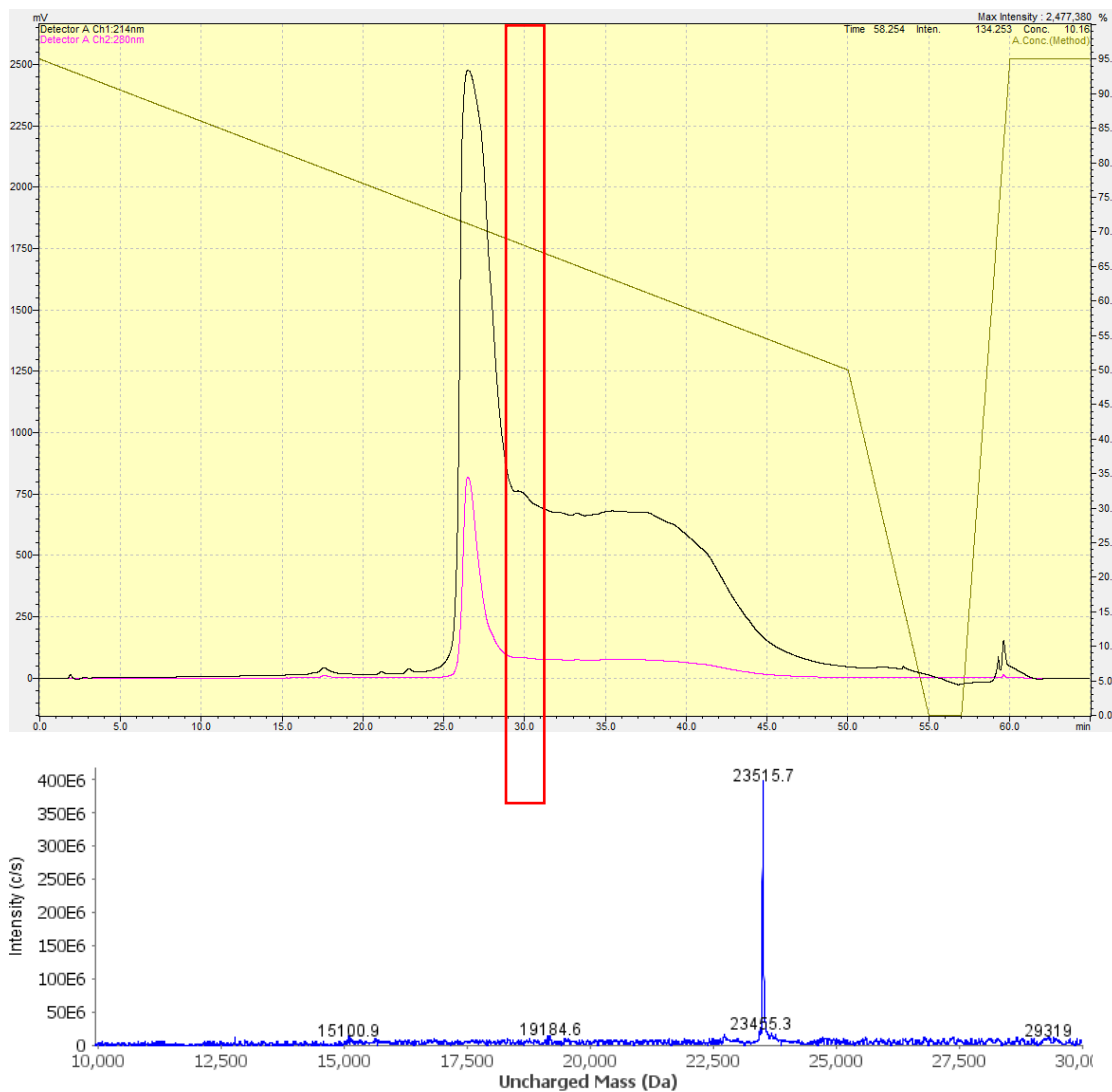


Figure S1: ^{15}N wild-type PrP with *p*-Acetyl-phenylalanine at positions 180 and 196. Only the main peak was selected (red box).

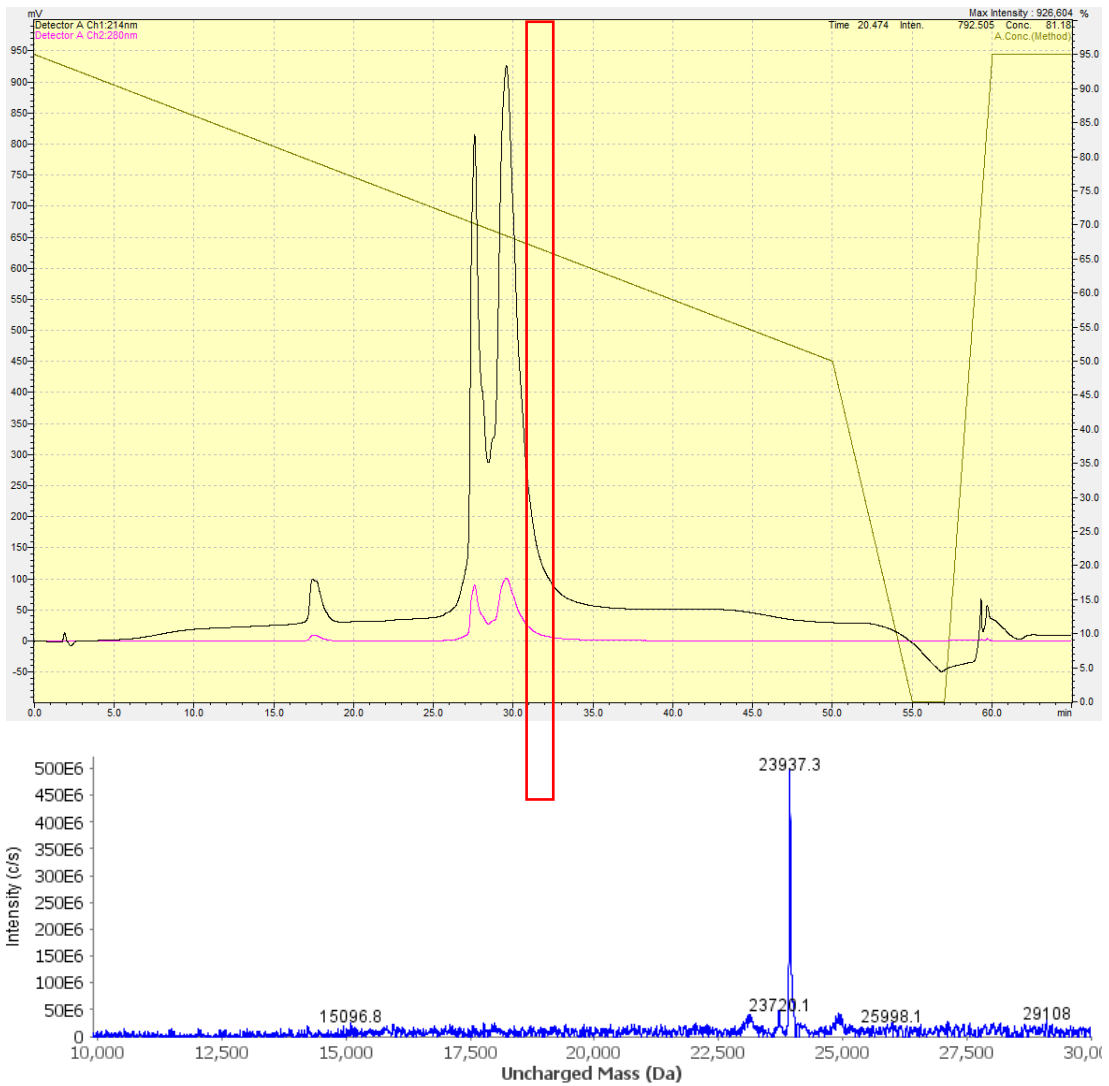


Figure S2: ^{15}N wild-type PrP with one-sugar-long glycans at positions 180 and 196. Only the first main peak was selected (red box).

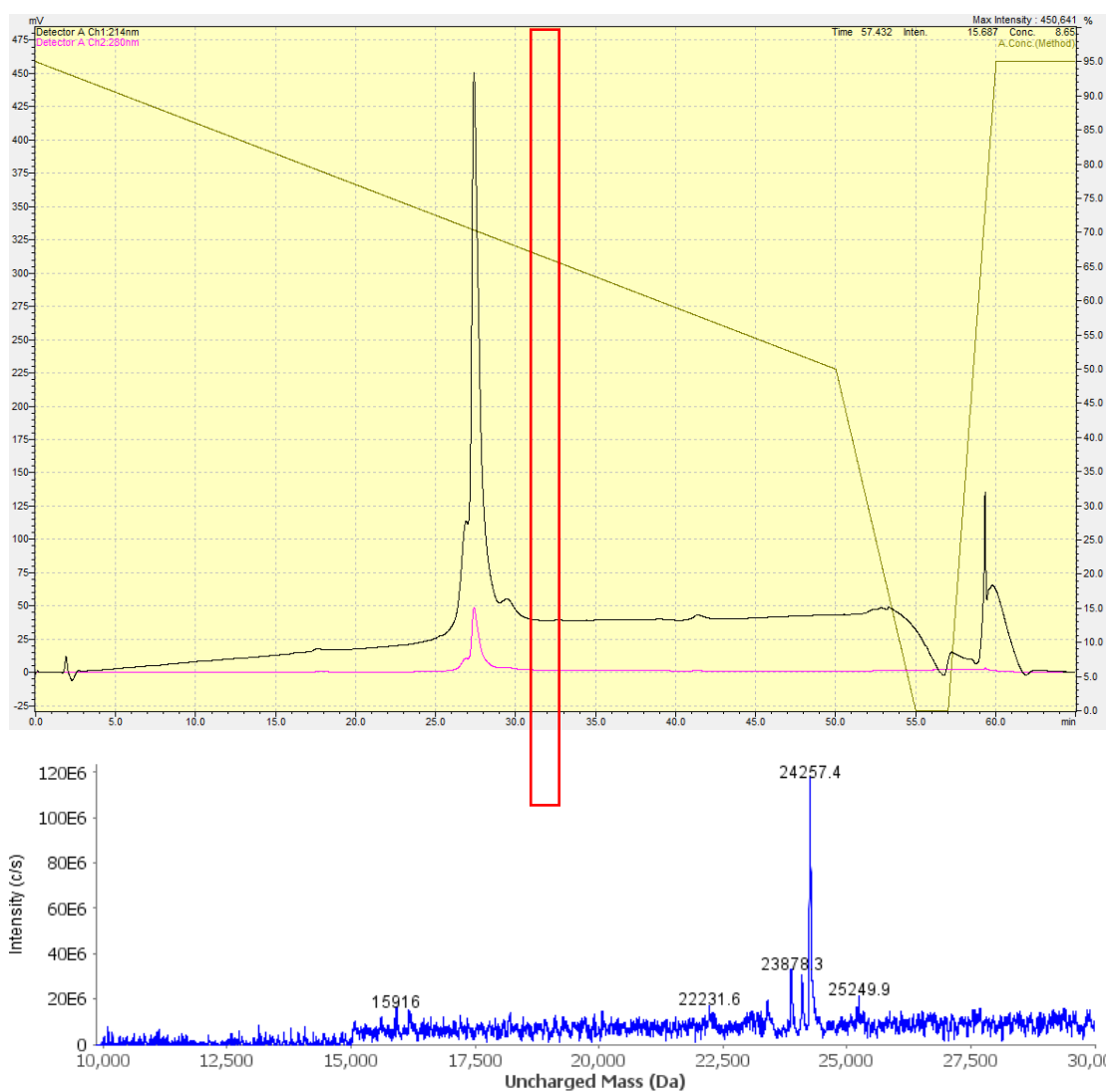


Figure S3: ^{15}N wild-type PrP with two-sugar-long glycans at positions 180 and 196. Only the center of the main peak was selected (red box).

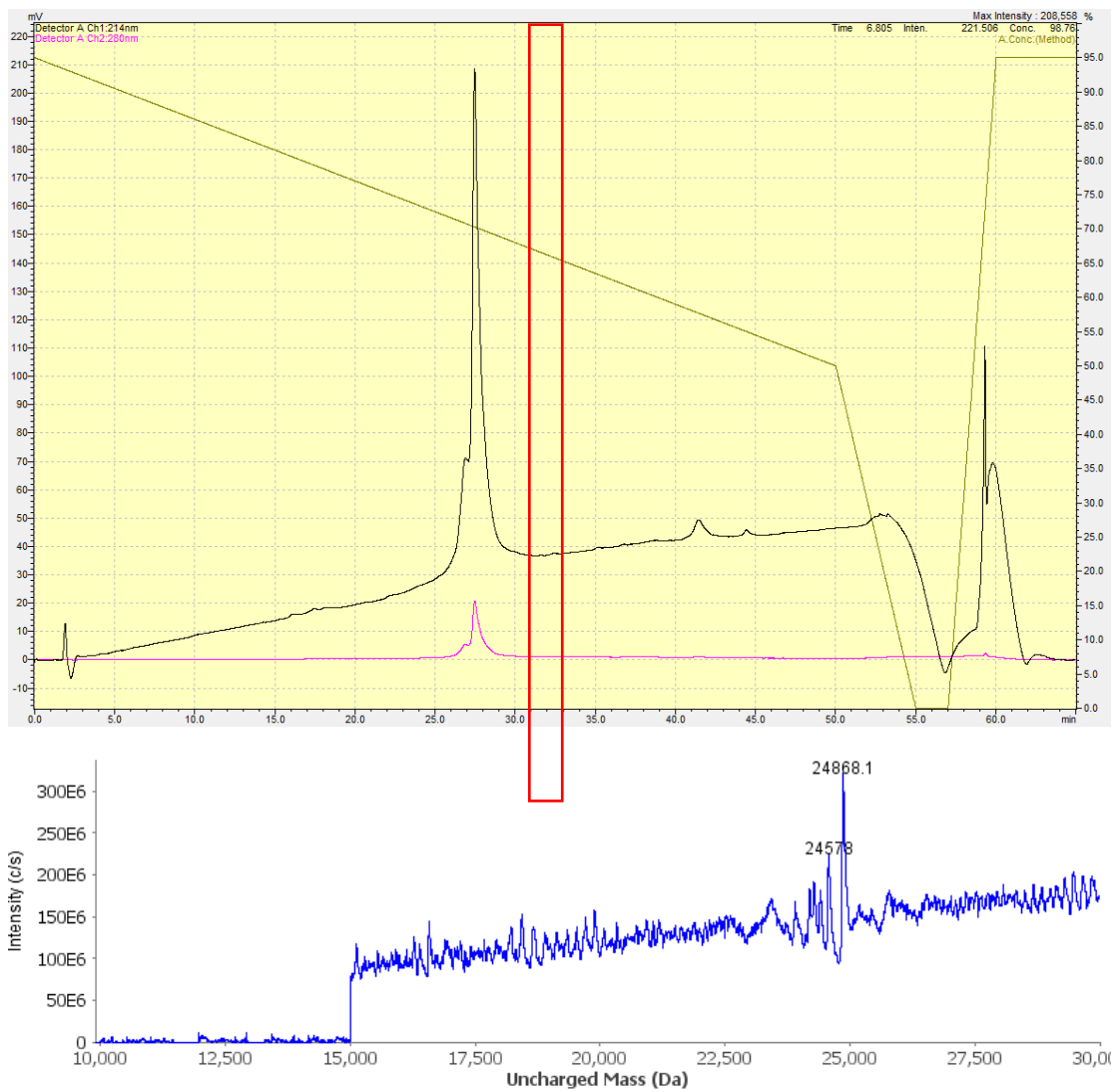


Figure S4: ^{15}N wild-type PrP with three-sugar-long glycans at positions 180 and 196. Only the center of the main peak was selected (red box).

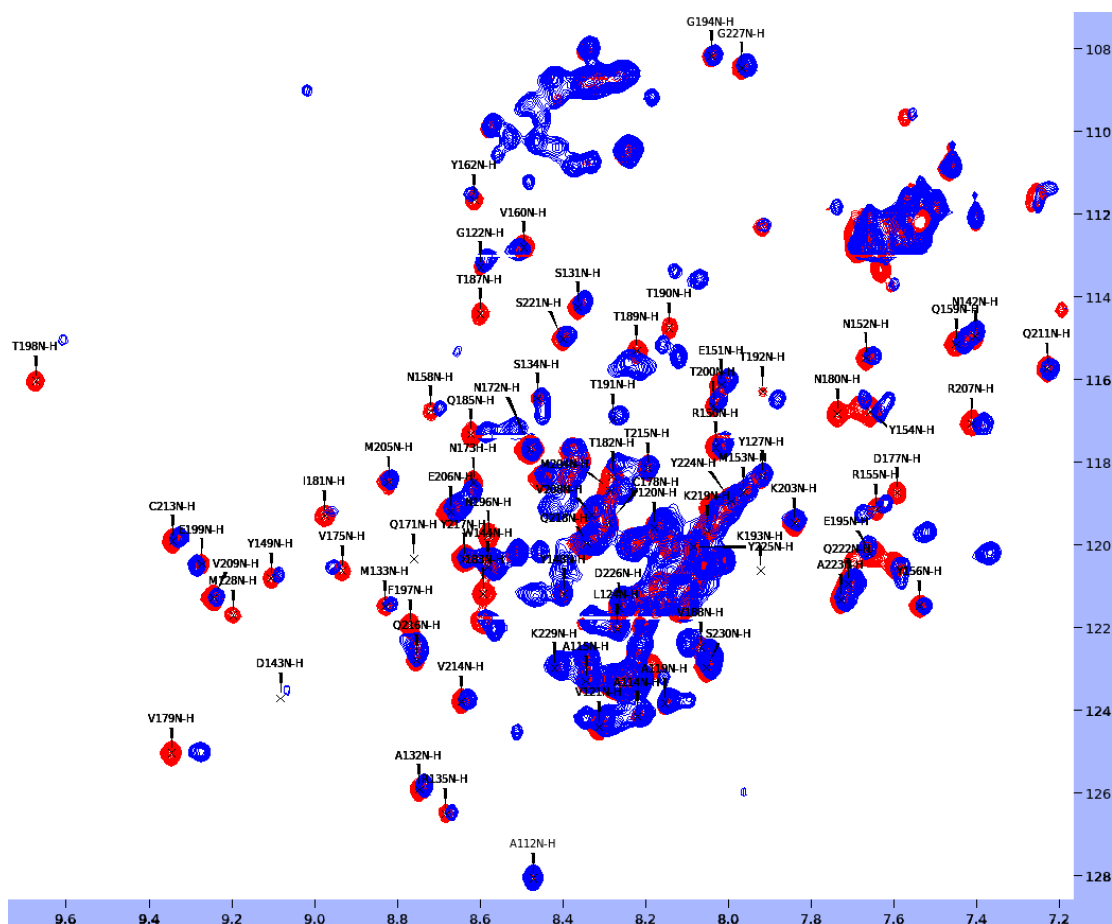


Figure S5: ^1H - ^{15}N HSQC NMR of wild-type PrP (red) and wild-type PrP with three-sugar-long glycans at positions 180 and 196 (blue). Labeled peaks with significant shifts (V179, T182, I183, Q185, T190, T191) are in close proximity to the glycans.

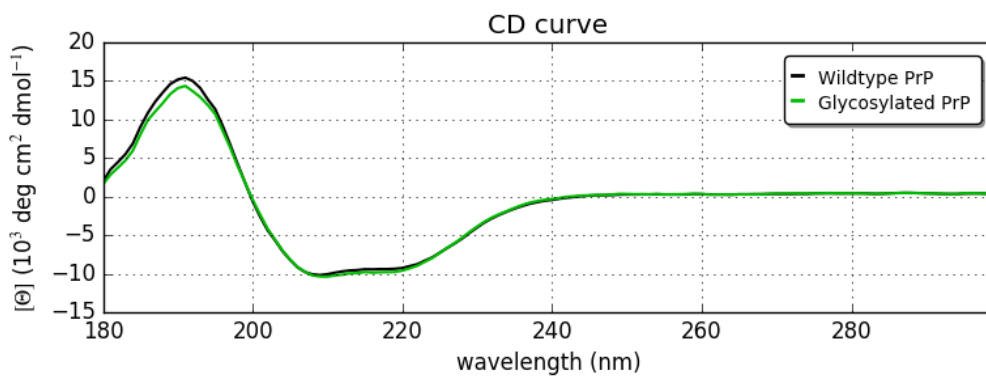


Figure S6: Circular dichroism spectra of wild-type and glycomimetic PrP.

minutes after buffer creation	pH of 100mM Acetic Acid, 200mM Ammonium Bicarbonate w/ stirring	pH of 200mM Acetic Acid, 200mM Ammonium Bicarbonate w/ stirring	pH of 100mM Acetic Acid, 300mM Ammonium Bicarbonate w/ stirring	pH of 100mM Acetic Acid, 200mM Ammonium Bicarbonate no stirring	pH of 200mM Acetic Acid, 200mM Ammonium Bicarbonate no stirring	pH of 100mM Acetic Acid, 300mM Ammonium Bicarbonate no stirring
5	6.5	5.73	6.85			
30	6.75	5.81	7.02			
60	7.09	5.9	7.35			
90	7.4	6	7.67			
120	7.65	6.1	7.85			
150	7.8	6.2	8			
180	7.88	6.21	8.14			
210	7.9	6.21	8.21			
240	8.02	6.25	8.22			
270	8.03	6.25	8.22			
1440	8.02	6.25	8.21			
5				6.5	5.73	6.85
60				6.79	5.89	7.08
180				6.84	5.89	7.13
300				6.84	5.91	7.17
420				6.91	5.92	7.24
540				7.01	5.96	7.38
780				7.06	5.98	7.49
1080				7.08	6.01	7.56
1440				7.1	6.03	7.62

Figure S7: Raw data of buffer pH vs time for various buffer concentrations, with and without stirring.

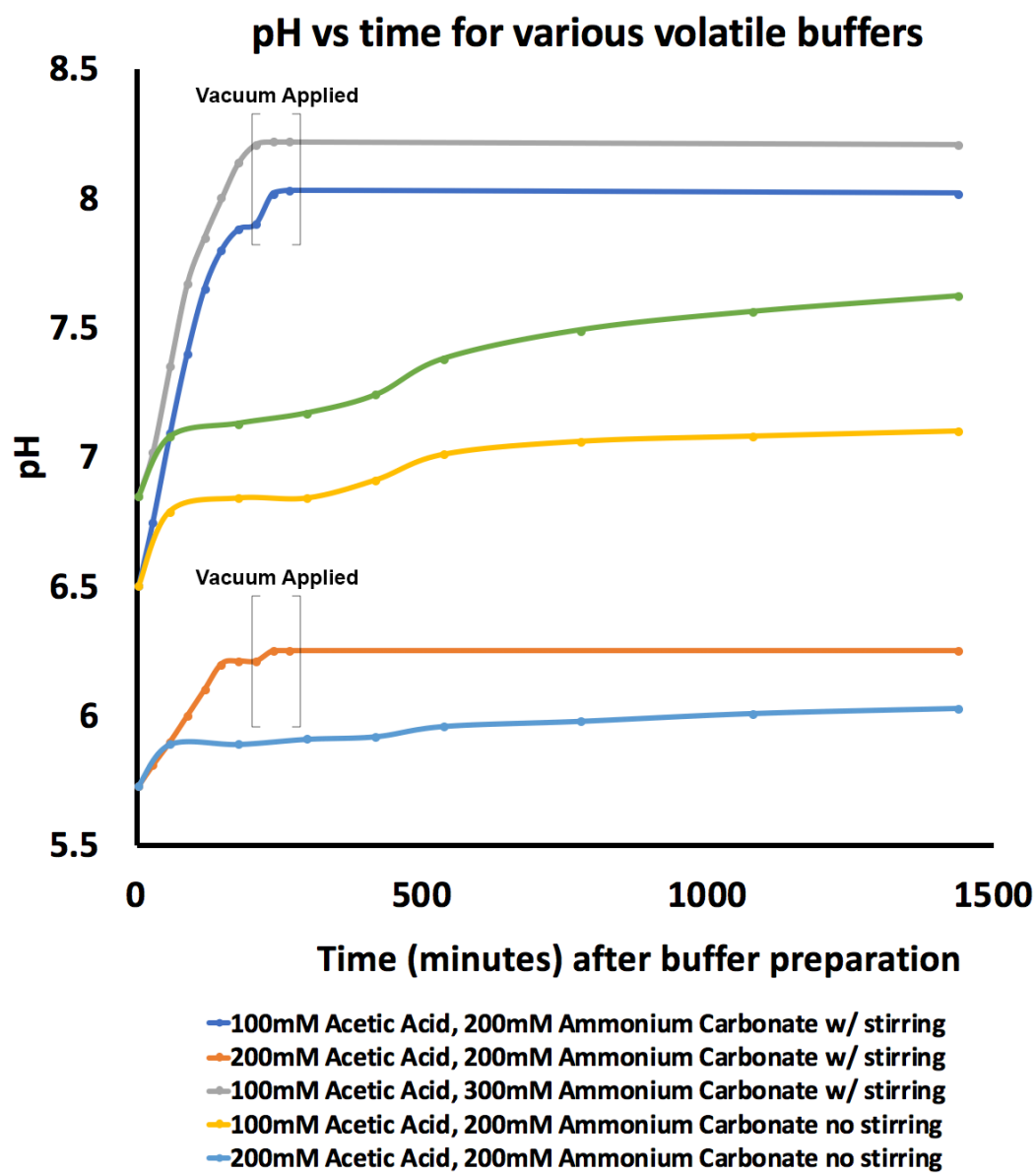


Figure S8: Change in pH over time of volatile buffer mixtures. With no stirring, the scan takes >24 hours, and with vigorous stirring the scan takes approximately three hours.

Chapter 4

The Prion Protein's Glycans Refine its Neuroprotective, Copper-Driven Self-Regulatory *Cis* Interaction

Introduction

PrP^C contains two N-linked glycosylation sites at asparagines 180 and 196, proximal to the location of many of its pathological mutations[71]. The protein exists as a mixture of unglycosylated, diglycosylated, and both possible monoglycosylated forms. Each glycan is varied in its molecular composition and size. Glycosylation status is not solely responsible for the encoding of prion strain information, but may contribute, as glycosylation status differs between strains [84-86]. The plaques in two human prion diseases, familial Creutzfeldt-Jakob disease caused by V180I and variably protease-sensitive prionopathy, contain PrP devoid of glycosylation at N181[87].

It is difficult to study the effects of glycosylation in a laboratory, because the only way to force certain glycosylation patterns is by mutating the amino acids that code for the glycans. This not only produces changes in glycosylation status, but changes in amino acids on the surface of the protein. There is evidence from mutant studies that prion glycoforms preferentially convert themselves more easily than they convert other glycoforms, but the amino acid changes in these studies must be considered as well[87,88] In other words, each prion glycoform of PrP^{Sc} converts certain glycoforms of PrP^C to PrP^{Sc} more easily than others, but because many laboratory experiments use amino acid mutations to enforce glycoforms, it is unclear whether these conversion preferences are due to differences in the status of the glycans, or to the differences in amino acids that coded for the status of the glycans. In a non-mutant study, prion strains preserved their glycoform ratios in *in vitro* conversion assays, suggesting that glycoforms do in fact have self-conversion preferences[89].

Strain specific neurotropism, the phenomenon in which strains preferentially affect certain regions of the brain, may be explained by the glycoform conversion preferences of strains, as PrP^C glycosylation also differs across brain regions[90-92].

We previously showed that two histidines on the C-terminus of the prion protein coordinate copper together with N-terminal histidines, driving a neuroprotective *cis* interaction between the two termini[93]. One of these residues, histidine 176, is one turn of an alpha helix away from the glycosylation site at asparagine 180 (mouse numbering). Given that certain prion diseases contain no glycosylation at this asparagine, we wondered if glycosylation contributed to the *cis* interaction. We were also concerned about the applicability of our results to the prion protein *in vivo*, given that the recombinant protein used was unglycosylated, and that glycans are fairly large and may sterically hinder the *cis* interaction. In this chapter, we use artificially glycosylated PrP^C to investigate the effects of the glycans on this neuroprotective self-regulatory interaction.

Using electron paramagnetic resonance (EPR), we show that glycans on PrP^C do not significantly inhibit or alter its copper binding modes. Using nuclear magnetic resonance (NMR), we show that the glycans refine the *cis* interaction, localizing the copper to a smaller area on the C-terminus of the protein. We also show that the glycans are capable of partially reversing the toxic loss of *cis* interaction caused by mutated C-terminal histidines.

Results

Glycans on the C-terminus of PrP^C do not significantly inhibit its copper binding.

Continuous wave EPR was used to probe the coordination environment of the copper bound to unglycosylated and artificially glycosylated PrP^C at pH 6. Both unglycosylated and glycosylated samples show spectra consistent with four equatorial nitrogen ligands (Figure 1). The parallel regions of the spectra, between 2600G and 3100G, are a perfect match, while the perpendicular regions match in multiplicity and field, with a slight difference in hyperfine signal intensity. Overall, these data show that glycans on the C-terminus of PrP^C do not inhibit or significantly alter its copper coordination modes.

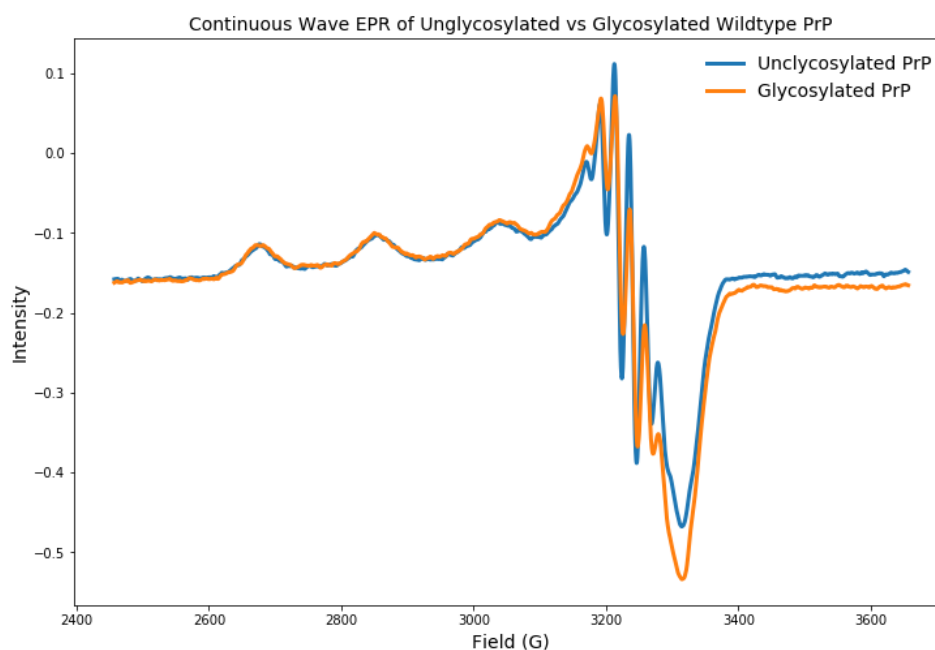


Figure 1. Continuous wave EPR showing the copper coordination environment in glycosylated and unglycosylated PrP.

Glycans on the C-terminus of the prion protein refine its *cis* interaction.

After confirming that glycosylated prion protein coordinates copper with four equatorial ligands in the same manner that unglycosylated prion protein does, we set out to discover if there were differences in where this coordination was occurring within the protein. We employed ^1H - ^{15}N HSQC NMR analysis on glycosylated and unglycosylated PrP^C at pH 6 to determine the approximate location of the copper on the C-terminus of the protein. As discussed in chapter 2, copper negatively affects the NMR signal intensity of nearby nuclei in a distance dependent manner, due to line broadening from paramagnetic relaxation enhancement (PRE).

We observed that the glycosylated prion protein had slightly weaker overall line broadening than the unglycosylated protein, but that this broadening was concentrated to a smaller area of the protein (Figure 2). Specifically, while the unglycosylated protein had significant line broadening around the areas of histidine 139 and histidine 176, the broadening in the glycosylated protein was focused mainly around histidine 176. This histidine is in close proximity to the glycans, being four residues (one helical turn) away from the glycan attached to asparagine 180. This suggests that the glycans are not sterically hindering the *cis* interaction, but are instead contributing to it positively. These data are shown in an absolute manner in Figure 2.

Because the artificially glycosylated protein is much larger than the unglycosylated protein, it tumbles more slowly in solution. This leads to lower overall signal intensity in NMR experiments, and may affect the amount of PRE derived line broadening that is observed from copper coordination. Therefore, although the line

broadening information displayed in Figure 2 shows us changes in location of the copper, it does not conclusively show that the strength of the *cis* interaction is reduced.

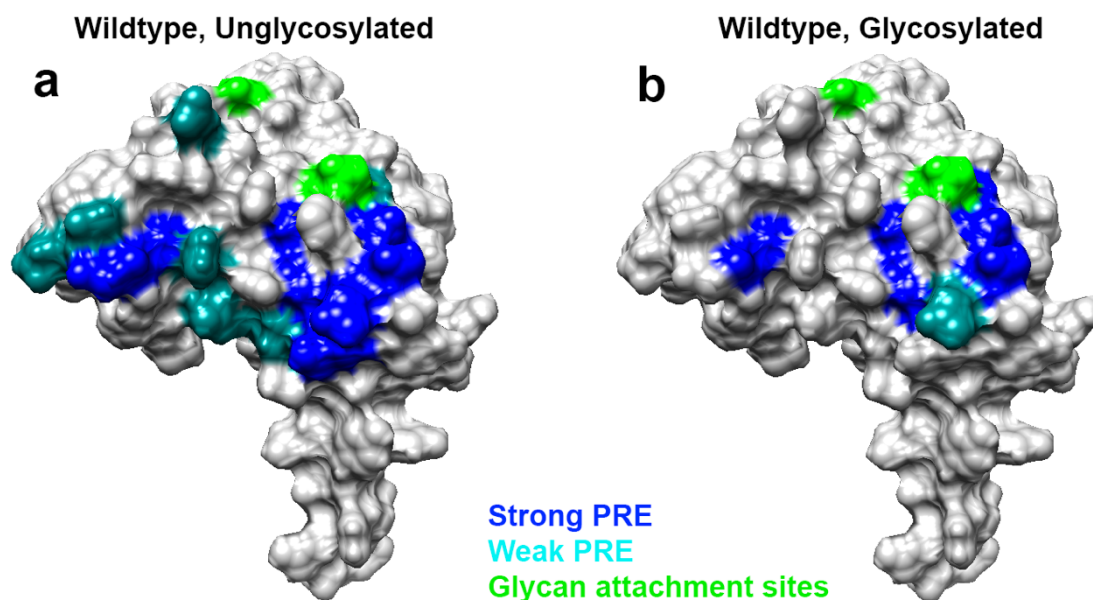


Figure 2. Surface representations showing areas of wild-type PrP^C engaged in the *cis* interaction, with and without glycans, as measured by the intensity reduction of NMR cross peaks. Plotted on PDB: 1XYX.

Although we cannot interpret the differences in the absolute strength of PRE derived line broadening between mutants of different molecular weights, we can compare the rank orders of residues broadened in each mutant. Because PRE line broadening occurs in a distance dependent fashion, we know that residues whose signals are the most broadened are the closest to the copper in space. We can compare the unglycosylated and glycosylated proteins in terms of which residues moved upwards or downwards in line broadening rank. This shows us movement in the time-averaged position of the coordinated copper. We observe that the addition of glycans

has caused the coordinated copper to move away from histidine 139, and closer to histidine 176, on average (Figure 3).

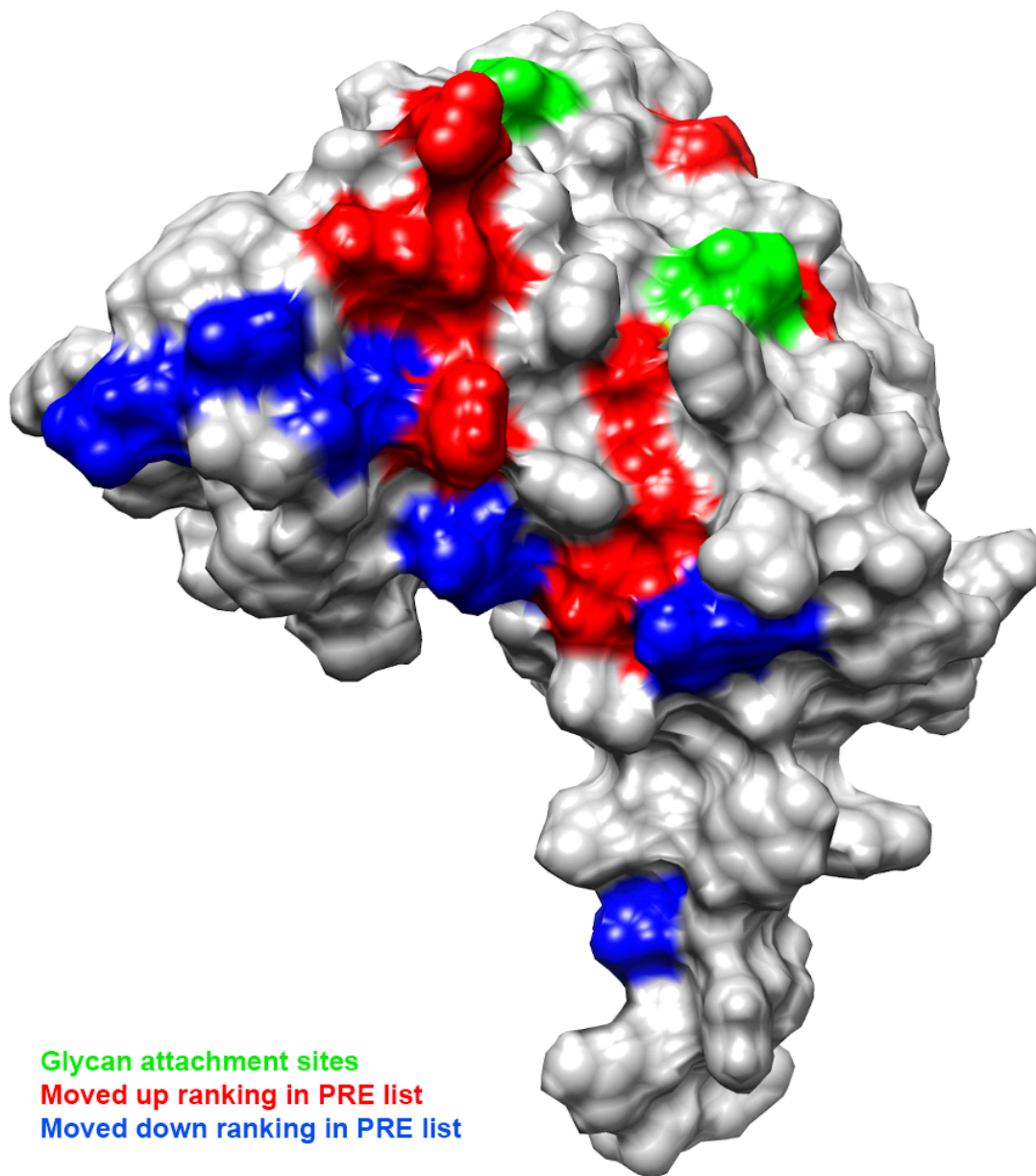


Figure 3. Surface representation showing the areas of wild-type PrP^C engaged in the *cis* interaction that change the most with the addition of glycans, as measured by the intensity reduction of NMR cross peaks. Plotted on PDB: 1XYX.

Glycans partially restore *cis* interaction lost by mutation of C-terminal histidines.

As discussed in chapter 2, two histidines on the C-terminus of PrP^C coordinate copper together with N-terminal histidines, driving a neuroprotective *cis* interaction through a molecular tether. When these histidines are mutated away, the interaction is lost and replaced with a much weaker interaction driven by a patch of negatively charged residues on the C-terminus. By performing ¹H-¹⁵N HSQC NMR analysis on glycosylated and unglycosylated (H13Y, H176Y) PrP^C at pH 6, we show that the glycans partially restore the lost interaction. Specifically, whereas the unglycosylated wild-type protein has strong copper coordination around both histidines 139 and 176, the glycosylated and histidine-mutated protein has strong copper coordination around the former location of histidine 176 only (Figure 4). This suggests that the *cis* interaction in the cellular version of the protein may be exclusively between the N-terminal histidines and histidine 176, and is assisted by the nearby glycans.

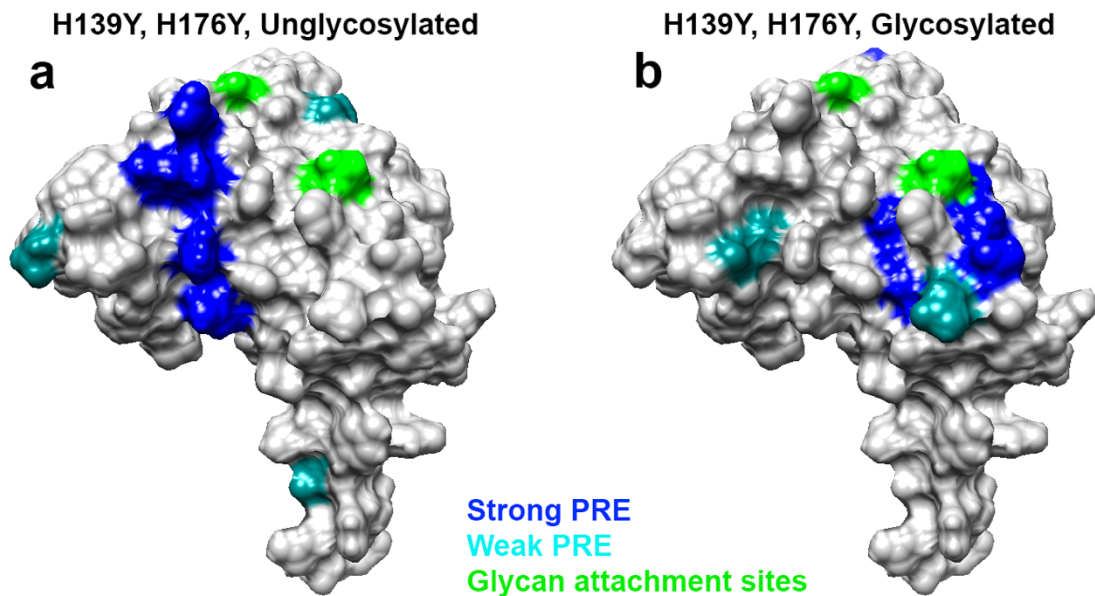


Figure 4. Surface representations showing areas of H139Y, H176Y PrP^C engaged in the *cis* interaction, with and without glycans, as measured by the intensity reduction of NMR cross peaks. Plotted on PDB: 1XYX.

Discussion

In this study we show that glycans on the C-terminus of PrP^C refine the proteins neuroprotective, copper-driven *cis* interaction, localizing it to a smaller region on the protein. We also show that the glycans partially rescue a toxic loss of this interaction caused by the mutation of C-terminal histidines. Together, these results suggest that the glycans contribute structurally to a self-regulation in wild-type protein. The glycan located at N180 is much closer to the previously determined site of the *cis* interaction than the glycan at N196, and we have not investigated them separately. It is possible that only one of the glycans is responsible for the effects observed in the study reported in chapter, and future work will further examine this question. Future work will also be

done to investigate whether glycans can reverse toxicity caused by mutated C-terminal histidines in cell culture. The glycosylated protein used in this study was artificially glycosylated, with the trisaccharide N-acetylglucosamine, galactose, sialic acid. The glycans in real PrP^C are larger and more diverse in composition, and this difference needs to be considered when interpreting this study.

Materials and Methods

Protein Preparation

The protein used for the experiments in this in this chapter was produced using protocol given in chapter 3[94]. Briefly, plasmids containing the genes for PrP and the necessary machinery to incorporate *p*-acetyl-phenylalanine were transformed into *E.coli*. The bacteria was grown in minimal media with ¹⁵N ammonium chloride and *p*-acetyl-phenylalanine added, producing PrP with two *p*-acetyl-phenylalanine residues at the locations of the glycan attachment points. The protein was purified by nickel affinity chromatography and reverse phase high performance liquid chromatography (HPLC). The protein was allowed to react with aminoxy N-Acetylglucosamine, which attached to the two *p*-acetyl-phenylalanines through oxime linkages. Glycosyltransferases were then used to extend these sugar into trisaccharides, and the protein was once again purified by HPLC. The resulting protein was glycosylated at both residues 180 and 196 with the trisaccharide N-acetylglucosamine, galactose, sialic acid.

Electron Paramagnetic Resonance Spectroscopy

All samples were made to pH 6.0 in 50 mM 2-(*N*-morpholino)ethanesulfonic acid (MES) buffer (Sigma), using potassium as a counterion. The protein was added to a concentration of 100 μ M, and CuCl₂ was used at 100 μ M. The samples contained 30% glycerol as a cryoprotectant. X-band (9.38 GHz) continuous-wave (CW) EPR spectra were recorded on a Bruker (Billerica, MA) EleXsys E580 spectrometer equipped with a super-high Q resonator (ER4122SHQE). Cryogenic temperatures were achieved with a liquid nitrogen finger dewar and gas flow controller. The spectrometer settings were as follows: temperature = 121 K, conversion time = 41 ms, modulation amplitude = 0.5 mT, modulation frequency = 100 kHz, bridge power = 5 mW, attenuation = 23 dB.

Nuclear Magnetic Resonance Spectroscopy

All samples were made to pH 6.0 in 10 mM 2-(*N*-morpholino)ethanesulfonic acid (MES) buffer (Sigma), using potassium as a counterion and containing 10% D₂O. For all samples, the protein was added to a concentration of 100 μ M. For samples with copper, CuCl₂ was used at 100 μ M. ¹H-¹⁵N HSQC spectra were recorded at 37 °C on a Bruker 800 MHz spectrometer at the UCSC NMR facility. NMR spectra were analyzed with NMR Pipe and Sparky using assignments transferred from previous experiments by visual inspection, and figures were made using Chimera, R, and python. To determine a cutoff i/i_0 value to separate the residues involved in the *cis* interaction from the rest of the protein, we performed a kernel density estimation on the data using a Gaussian smoothing kernel. To eliminate the effects of differential unspecific peak

intensity reduction across mutants, the data were scaled so that the center values of each mutant's group of unaffected peaks were aligned. We divided the residues into three categories based on their i/i_0 values: strongly affected (dark blue), weakly affected (light blue) and unaffected (grey). These divisions were created by using the local minimum separating the affected from unaffected residues in the wild-type protein ($i/i_0 = 0.35$), and dividing the affected peaks into two groups ($i/i_0 = 0$ to 0.175 , and $i/i_0 = 0.175$ to 0.35).

Acknowledgements

We thank NIH grants R01GM065790 and R35GM131781 for financial support, and NIH instrumentation grant S10OD018455 for acquisition of the 800 MHz NMR spectrometer. We also thank Drs. K. Sakamoto and S. Yokoyama at the RIKEN Yokohama branch for providing the B-95.AAAfabR *E.coli* strain. Dr. Tufa Assafa performed the EPR experiments in this chapter.

Chapter 5

Conclusions

Conclusions

This dissertation contains two central findings and one method development. We first find that two C-terminal histidines bind copper together with N-terminal histidines, driving a neuroprotective self-regulatory *cis* interaction between the two domains of the protein. Removal of these histidines inhibits the *cis* interaction, and leads to toxic spontaneous currents in cell culture – a sign of prion-like toxicity. We use these findings to propose a mechanism of action for a class of genetic prion diseases – the octarepeat deletion disorders, and show NMR data supporting this claim. We then develop a method to create artificially, doubly glycosylated, ¹⁵N labelled prion protein, with a volatile, pH-scanning buffer as a sub development. Lastly, we use this glycosylated protein to investigate the effects of glycans on the *cis* interaction. We find that the glycans refine the *cis* interaction, localizing it to a narrower region on the C-terminus of the protein. In addition, the glycans partially restore the toxic loss of *cis* interaction caused by mutated C-terminal histidines, suggesting a neuroprotective role for the glycans.

Together, these results show that at least two molecular factors contribute to the prion proteins neuroprotective *cis* interaction – C-terminal histidines, and C-terminal glycans. A patch of negatively charged amino acids is a third possible contributor, located in the same general region as the histidines and glycans, and previously implicated in the *cis* interaction[15,18]. Out of these three contributors, the histidines are capable of the strongest coordination to copper, but are small and remain close to the surface of the protein. The negatively charged residues, three glutamates and one

aspartate, are much less strongly attracted to copper than is histidine, but there are four of these residues situated midway between the two histidines. The glycans are even less strongly attracted to copper, containing only one negative charge at their capping saccharide sialic acid and an abundance of lone paired oxygen atoms throughout, but are much larger in volume than either the histidines or negatively charged residues. The N-terminus of PrP^C is long and unstructured, creating a large conformational entropy penalty for interaction with the C-terminus.

We propose a chain of events involving all contributors to the *cis* interaction, although we do not have evidence that these events occur in a sequence. First, copper binds strongly to three or four N-terminal histidines. The copper bound N-terminus samples conformational space until it encounters glycans, which are large and extend far away from the C-terminus. The interaction between the glycans and copper biases the N-terminus towards conformations close to the C-terminus. Within these limited conformations, the copper bound N-terminus encounters the four negatively charged amino acids on the surface of the protein, forming favorable interactions and further reducing conformational space. Lastly, the copper bound N-terminus encounters and binds strongly to C-terminal histidines, locking in the *cis* interaction with an energetically favorable coordination (Figure 1). There is therapeutic potential in strengthening this interaction in order to make the protein more resistant to misfolding and toxicity. Further work needs to be done in order to determine whether or not there is a preference for one C-terminal histidine, as well as whether or not both glycans contribute to the *cis* interaction equally.

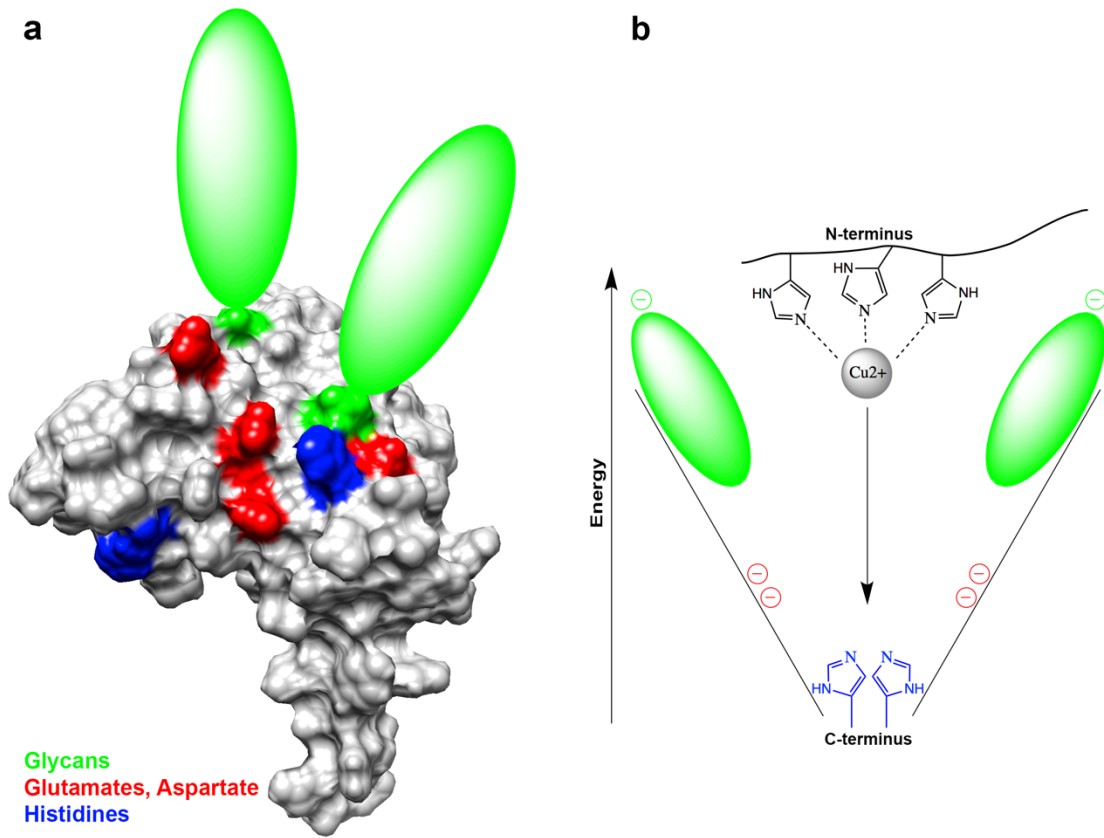


Figure 1. Unified model showing three contributors to the *cis* interaction in PrP^C. Plotted on PDB: 1XYX.

References

- [1] S.B. Prusiner, Novel proteinaceous infectious particles cause scrapie, *Science*. 216 (1982) 136–144.
- [2] S.B. Prusiner, Prions, *Proceedings of the National Academy of Sciences*. 95 (1998) 13363–13383. doi:10.1073/pnas.95.23.13363.
- [3] D. Riesner, Biochemistry and structure of PrP(C) and PrP(Sc), *Br. Med. Bull.* 66 (2003) 21–33. doi:10.1093/bmb/66.1.21.
- [4] H. Wille, J. Requena, The Structure of PrPSc Prions, *Pathogens*. 7 (2018) 20–11. doi:10.3390/pathogens7010020.
- [5] G.R. Mallucci, S. Ratté, E.A. Asante, J. Linehan, I. Gowland, J.G.R. Jefferys, et al., Post-natal knockout of prion protein alters hippocampal CA1 properties, but does not result in neurodegeneration, *The EMBO Journal*. 21 (2002) 202–210. doi:10.1093/emboj/21.3.202.
- [6] E. Biasini, J.A. Turnbaugh, U. Unterberger, D.A. Harris, Prion protein at the crossroads of physiology and disease, *Trends in Neurosciences*. 35 (2012) 92–103. doi:10.1016/j.tins.2011.10.002.
- [7] S. Brandner, S. Isenmann, A. Raeber, M. Fischer, A. Sailer, Y. Kobayashi, et al., Normal host prion protein necessary for scrapie-induced neurotoxicity, *Nature*. 379 (1996) 339–343. doi:10.1038/379339a0.
- [8] B. Chesebro, M. Trifilo, R. Race, K. Meade-White, C. Teng, R. LaCasse, et al., Anchorless prion protein results in infectious amyloid disease without clinical scrapie, *Science*. 308 (2005) 1435–1439. doi:10.1126/science.1110837.
- [9] G. Mallucci, A. Dickinson, J. Linehan, P.-C. Klöhn, S. Brandner, J. Collinge, Depleting neuronal PrP in prion infection prevents disease and reverses spongiosis, *Science*. 302 (2003) 871–874. doi:10.1126/science.1090187.
- [10] A. Li, H.M. Christensen, L.R. Stewart, K.A. Roth, R. Chiesa, D.A. Harris, Neonatal lethality in transgenic mice expressing prion protein with a

- deletion of residues 105–125, *The EMBO Journal*. 26 (2007) 548–558. doi:10.1038/sj.emboj.7601507.
- [11] B. Wu, A.J. McDonald, K. Markham, C.B. Rich, K.P. Mchugh, The N-terminus of the prion protein is a toxic effector regulated by the C-terminus, *eLife*. (2017). doi:10.7554/eLife.23473.001.
- [12] R.R. Reimann, T. Sonati, S. Hornemann, U.S. Herrmann, M. Arand, S. Hawke, et al., Differential Toxicity of Antibodies to the Prion Protein, *PLoS Pathog*. 12 (2016) e1005401–19. doi:10.1371/journal.ppat.1005401.
- [13] I.H. Solomon, J.E. Huettner, D.A. Harris, Neurotoxic mutants of the prion protein induce spontaneous ionic currents in cultured cells, *J. Biol. Chem*. 285 (2010) 26719–26726. doi:10.1074/jbc.M110.134619.
- [14] T. Sonati, R.R. Reimann, J. Falsig, P.K. Baral, T. O'Connor, S. Hornemann, et al., The toxicity of anti-prion antibodies is mediated by the flexible tail of the prion protein, *Nature*. 501 (2013) 102–106. doi:10.1038/nature12402.
- [15] A.R. Spevacek, E.G.B. Evans, J.L. Miller, H.C. Meyer, J.G. Pelton, G.L. Millhauser, Zinc drives a tertiary fold in the prion protein with familial disease mutation sites at the interface, *Structure*. 21 (2013) 236–246. doi:10.1016/j.str.2012.12.002.
- [16] L. Shen, H.-F. Ji, Mutation directional selection sheds light on prion pathogenesis, *Biochemical and Biophysical Research Communications*. 410 (2011) 159–163. doi:10.1016/j.bbrc.2011.06.007.
- [17] A.K. Thakur, A.K. Srivastava, V. Srinivas, Copper alters aggregation behavior of prion protein and induces novel interactions between its N- and C-terminal regions, *Journal of Biological Chemistry*. 286 (2011) 38533–38545. doi:10.1074/jbc.m111.265645.
- [18] E.G.B. Evans, M.J. Pushie, K.A. Markham, H.-W. Lee, G.L. Millhauser, Interaction between Prion Protein's Copper-Bound Octarepeat Domain and a Charged C-Terminal Pocket Suggests a Mechanism for N-Terminal Regulation, *Structure/Folding and Design*. 24 (2016) 1057–1067. doi:10.1016/j.str.2016.04.017.

- [19] J.R. Silveira, G.J. Raymond, A.G. Hughson, R.E. Race, V.L. Sim, S.F. Hayes, et al., The most infectious prion protein particles, *Nature*. 437 (2005) 257–261. doi:10.1038/nature03989.
- [20] J. Masel, N. Genoud, A. Aguzzi, Efficient Inhibition of Prion Replication by PrP-Fc2 Suggests that the Prion is a PrPSc Oligomer, *Journal of Molecular Biology*. 345 (2005) 1243–1251. doi:10.1016/j.jmb.2004.10.088.
- [21] A.J. McDonald, D.R. Leon, K.A. Markham, B. Wu, C.F. Heckendorf, K. Schilling, et al., Altered Domain Structure of the Prion Protein Caused by Cu²⁺ Binding and Functionally Relevant Mutations: Analysis by Cross-Linking, MS/MS, and NMR, *Structure/Folding and Design*. 27 (2019) 907–922.e5. doi:10.1016/j.str.2019.03.008.
- [22] M.J. Pushie, I.J. Pickering, G.R. Martin, S. Tsutsui, F.R. Jirik, G.N. George, Prion protein expression level alters regional copper, iron and zinc content in the mouse brain, *Metallomics*. 3 (2011) 206–9. doi:10.1039/c0mt00037j.
- [23] A.D. Armendariz, M. Gonzalez, A.V. Loguinov, C.D. Vulpe, Gene expression profiling in chronic copper overload reveals upregulation of Prnp and App, *Physiological Genomics*. 20 (2004) 45–54. doi:10.1152/physiolgenomics.00196.2003.
- [24] L. Varela-Nallar, E.M. Toledo, L.F. Larrondo, A.L.B. Cabral, V.R. Martins, N.C. Inestrosa, Induction of cellular prion protein gene expression by copper in neurons, *American Journal of Physiology-Cell Physiology*. 290 (2006) C271–C281. doi:10.1152/ajpcell.00160.2005.
- [25] R. Linden, V.R. Martins, M.A.M. Prado, M. Cammarota, I. Izquierdo, R.R. Brentani, Physiology of the Prion Protein, *Physiological Reviews*. 88 (2008) 673–728. doi:10.1152/physrev.00007.2007.
- [26] E. Aronoff-Spencer, C.S. Burns, N.I. Avdievich, G.J. Gerfen, J. Peisach, W.E. Antholine, et al., Identification of the Cu²⁺ Binding Sites in the N-Terminal Domain of the Prion Protein by EPR and CD Spectroscopy †, *Biochemistry*. 39 (2000) 13760–13771. doi:10.1021/bi001472t.
- [27] C.S. Burns, E. Aronoff-Spencer, G. Legname, S.B. Prusiner, W.E. Antholine, G.J. Gerfen, et al., Copper coordination in the full-length,

- recombinant prion protein, *Biochemistry*. 42 (2003) 6794–6803. doi:10.1021/bi027138.
- [28] C.S. Burns, E. Aronoff-Spencer, C.M. Dunham, P.L. Biochemistry, 2002, Molecular features of the copper binding sites in the octarepeat domain of the prion protein, ACS Publications. 41 (2002) 3991–4001. doi:10.1021/bi011922x.
- [29] M. Chattopadhyay, E.D. Walter, D.J. Newell, P.J. Jackson, E. Aronoff-Spencer, J. Peisach, et al., The Octarepeat Domain of the Prion Protein Binds Cu(II) with Three Distinct Coordination Modes at pH 7.4, *J. Am. Chem. Soc.* 127 (2005) 12647–12656. doi:10.1021/ja053254z.
- [30] G.S. Jackson, I. Murray, L.L. Hosszu, N. Gibbs, J.P. Waltho, A.R. Clarke, et al., Location and properties of metal-binding sites on the human prion protein, *Proceedings of the National Academy of Sciences*. 98 (2001) 8531–8535. doi:10.1073/pnas.151038498.
- [31] G. Salzano, G. Giachin, G. Legname, Structural Consequences of Copper Binding to the Prion Protein, *Cells*. 8 (2019) 770–17. doi:10.3390/cells8080770.
- [32] G.L. Millhauser, Copper Binding in the Prion Protein †, *Acc. Chem. Res.* 37 (2004) 79–85. doi:10.1021/ar0301678.
- [33] C.G. Dudzik, E.D. Walter, B.S. Abrams, M.S. Jurica, G.L. Millhauser, Coordination of Copper to the Membrane-Bound Form of α -Synuclein, *Biochemistry*. 52 (2012) 53–60. doi:10.1021/bi301475q.
- [34] E.D. Walter, D.J. Stevens, A.R. Spevacek, M.P. Visconte, A. Dei Rossi, G.L. Millhauser, Copper binding extrinsic to the octarepeat region in the prion protein, *Curr. Protein Pept. Sci.* 10 (2009) 529–535.
- [35] S.A. Dikanov, A.P. Spoyalov, J. Hüttermann, Exploiting the properties of line-shape singularities in orientationally selected electron spin echo envelope modulation spectra of Cu^{2+} -(^{15}N -imidazole) 4for the determination of hyperfine coupling with the remote imidazole nitrogen, *The Journal of Chemical Physics*. 100 (1994) 7973–7983. doi:10.1063/1.466790.

- [36] T. Iwasaki, A. Kounosu, T. Uzawa, R.I. Samoilova, S.A. Dikanov, Orientation-Selected ^{15}N -HYSCORE Detection of Weakly Coupled Nitrogens around the Archaeal Rieske [2Fe–2S] Center, *J. Am. Chem. Soc.* 126 (2004) 13902–13903. doi:10.1021/ja045898x.
- [37] A.J. Hoff, *Advanced EPR Applications in Biochemistry and Biology*, 1989.
- [38] D. Getz, B.L. Silver, ESR of $\text{Cu}^{2+}(\text{H}_2\text{O})_6$. I. The oxygen-17 superhyperfine tensors in $^{63}\text{Cu}^{2+}$ doped zinc Tutton's salt at 20 °K, *The Journal of Chemical Physics*. 61 (1974) 630–637. doi:10.1063/1.1681939.
- [39] D. Kim, N.H. Kim, S.H. Kim, 34 GHz Pulsed ENDOR Characterization of the Copper Coordination of an Amyloid β Peptide Relevant to Alzheimer's Disease, *Angew. Chem. Int. Ed.* 52 (2012) 1139–1142. doi:10.1002/anie.201208108.
- [40] N.M. Atherton, A.J. Horsewill, Proton ENDOR of $\text{Cu}(\text{H}_2\text{O})_6^{2+}$ in $\text{Mg}(\text{NH}_4)_2(\text{SO}_4)_4 \cdot 6\text{H}_2\text{O}$, *Molecular Physics*. 37 (2006) 1349–1361. doi:10.1080/00268977900100991.
- [41] D.J. Stevens, E.D. Walter, A. Rodríguez, D. Draper, P. Davies, D.R. Brown, et al., Early Onset Prion Disease from Octarepeat Expansion Correlates with Copper Binding Properties, *PLoS Pathog.* 5 (2009) e1000390–11. doi:10.1371/journal.ppat.1000390.
- [42] J.A. Beck, S. Mead, T.A. Campbell, A. Dickinson, D.P. Wientjens, E.A. Croes, et al., Two-octapeptide repeat deletion of prion protein associated with rapidly progressive dementia, *Neurology*. 57 (2001) 354–356. doi:10.1212/wnl.57.2.354.
- [43] S. Capellari, P. Parchi, B.D. Wolff, J. Campbell, R. Atkinson, D.M. Posey, et al., Creutzfeldt–Jakob disease associated with a deletion of two repeats in the prion protein gene, *Neurology*. 59 (2002) 1628–1630. doi:10.1212/01.WNL.0000035533.86833.28.
- [44] M. Piazza, T.W. Prior, P.S. Khalsa, B. Appleby, A case report of genetic prion disease with two different PRNP variants, *Mol Genet Genomic Med.* 8 (2020) 277–8. doi:10.1002/mgg3.1134.

- [45] S. Katayama, I. Nakase, Y. Yano, T. Murayama, Y. Nakata, K. Matsuzaki, et al., Effects of pyrenebutyrate on the translocation of arginine-rich cell-penetrating peptides through artificial membranes: Recruiting peptides to the membranes, dissipating liquid-ordered phases, and inducing curvature, *BBA - Biomembranes*. 1828 (2013) 2134–2142. doi:10.1016/j.bbamem.2013.05.016.
- [46] P. Guterstam, F. Madani, H. Hirose, T. Takeuchi, S. Futaki, S.E. Andaloussi, et al., Elucidating cell-penetrating peptide mechanisms of action for membrane interaction, cellular uptake, and translocation utilizing the hydrophobic counter-anion pyrenebutyrate, *BBA - Biomembranes*. 1788 (2009) 2509–2517. doi:10.1016/j.bbamem.2009.09.014.
- [47] F. Madani, S. Lindberg, Ü. Langel, S. Futaki, A. Gräslund, Mechanisms of Cellular Uptake of Cell-Penetrating Peptides, *Journal of Biophysics*. 2011 (2011) 1–10. doi:10.1155/2011/414729.
- [48] G.W. Canters, U. Kolczak, F. Armstrong, L.J.C. Jeuken, R. Camba, M. Sola, The effect of pH and ligand exchange on the redox properties of blue copper proteins, *Faraday Disc*. 116 (2000) 205–220. doi:10.1039/b003822i.
- [49] L. Banci, I. Bertini, F. Cantini, I.C. Felli, L. Gonnelli, N. Hadjiladis, et al., The Atx1-Ccc2 complex is a metal-mediated protein-protein interaction, *Nat Chem Biol*. 2 (2006) 367–368. doi:10.1038/nchembio797.
- [50] K.N. Chacón, J. Perkins, Z. Mathe, K. Alwan, E.N. Ho, M.N. Ucisik, et al., Trapping intermediates in metal transfer reactions of the CusCBAF export pump of *Escherichia coli*, *Communications Biology*. (2018) 1–11. doi:10.1038/s42003-018-0181-9.
- [51] A.P. Garnett, J.H. Viles, Copper binding to the octarepeats of the prion protein. Affinity, specificity, folding, and cooperativity: insights from circular dichroism, *Journal of Biological Chemistry*. 278 (2003) 6795–6802. doi:10.1074/jbc.M209280200.

- [52] K. Qin, Y. Yang, P. Mastrangelo, D. Westaway, Mapping Cu(II) Binding Sites in Prion Proteins by Diethyl Pyrocarbonate Modification and Matrix-assisted Laser Desorption Ionization-Time of Flight (MALDI-TOF) Mass Spectrometric Footprinting, *Journal of Biological Chemistry*. 277 (2002) 1981–1990. doi:10.1074/jbc.M108744200.
- [53] G.M. Cereghetti, A. Schweiger, R. Glockshuber, S. Van Doorslaer, Electron Paramagnetic Resonance Evidence for Binding of Cu²⁺ to the C-terminal Domain of the Murine Prion Protein, *Biophys. J.* 81 (2001) 516–525. doi:10.1016/S0006-3495(01)75718-9.
- [54] M.C. Colombo, J. VandeVondele, S. Van Doorslaer, A. Laio, L. Guidoni, U. Rothlisberger, Copper binding sites in the C-terminal domain of mouse prion protein: A hybrid (QM/MM) molecular dynamics study, *Proteins*. 70 (2007) 1084–1098. doi:10.1002/prot.21604.
- [55] S. Van Doorslaer, G.M. Cereghetti, R. Glockshuber, A. Schweiger, Unraveling the Cu²⁺ Binding Sites in the C-Terminal Domain of the Murine Prion Protein: A Pulse EPR and ENDOR Study †, *J. Phys. Chem. B*. 105 (2001) 1631–1639. doi:10.1021/jp003115y.
- [56] S. Van Doorslaer, E. Vinck, The strength of EPR and ENDOR techniques in revealing structure–function relationships in metalloproteins, *Phys. Chem. Chem. Phys.* 9 (2007) 4620–19. doi:10.1039/b701568b.
- [57] S. Stoll, A. Schweiger, EasySpin, a comprehensive software package for spectral simulation and analysis in EPR, *Journal of Magnetic Resonance*. 178 (2006) 42–55. doi:10.1016/j.jmr.2005.08.013.
- [58] S. Stoll, R.D. Britt, General and efficient simulation of pulse EPR spectra, *Phys. Chem. Chem. Phys.* 11 (2009) 6614–14. doi:10.1039/b907277b.
- [59] W.B. Mims, Pulsed Endor Experiments, *Proceedings of the Royal Society a: Mathematical, Physical and Engineering Sciences*. 283 (1965) 452–457. doi:10.1098/rspa.1965.0034.
- [60] E.R. Davies, A new pulse endor technique, *Physics Letters A*. 47 (1974) 1–2. doi:10.1016/0375-9601(74)90078-4.

- [61] W. Bruggemann, J.R. Niklas, Stochastic ENDOR, *Journal of Magnetic Resonance, Series A*. 108 (1994) 25–29. doi:10.1006/jmra.1994.1084.
- [62] A.D. Gossert, S. Bonjour, D.L.P.O. the, 2005, Prion protein NMR structures of elk and of mouse/elk hybrids, *National Acad Sciences*. (n.d.).
- [63] M.J. Pushie, H.J. Vogel, Modeling by Assembly and Molecular Dynamics Simulations of the Low Cu^{2+} Occupancy Form of the Mammalian Prion Protein Octarepeat Region: Gaining Insight into Cu^{2+} -Mediated b-Cleavage, *Biophys. J.* 95 (2008) 5084–5091. doi:10.1529/biophysj.108.139568.
- [64] M.J. Pushie, K.H. Nienaber, A. McDonald, G.L. Millhauser, G.N. George, Combined EXAFS and DFT Structure Calculations Provide Structural Insights into the 1:1 Multi-Histidine Complexes of Cu II, Cu I, and Zn II with the Tandem Octarepeats of the Mammalian Prion Protein, *Chem. Eur. J.* 20 (2014) 9770–9783. doi:10.1002/chem.201304201.
- [65] M.J. Abraham, T. Murtola, R. Schulz, S. Páll, J.C. Smith, B. Hess, et al., GROMACS: High performance molecular simulations through multi-level parallelism from laptops to supercomputers, *SoftwareX*. 1-2 (2015) 19–25. doi:10.1016/j.softx.2015.06.001.
- [66] W.L. Jorgensen, D.S. Maxwell, J. Tirado-Rives, Development and Testing of the OPLS All-Atom Force Field on Conformational Energetics and Properties of Organic Liquids, *J. Am. Chem. Soc.* 118 (1996) 11225–11236. doi:10.1021/ja9621760.
- [67] M.J. Frisch, G.W. Trucks, H.B. Schlegel, G.E. Scuseria, M.A. Robb, J.R. Cheeseman, et al., *Gaussian 16 Rev. A.03*, (2016).
- [68] A.D. Becke, 1996, Density-functional thermochemistry. III. The role of exact exchange, *J. Chem Phys*, 1993.
- [69] S. Grimme, J. Antony, S. Ehrlich, H. Krieg, A consistent and accurate ab initio parametrization of density functional dispersion correction (DFT-D) for the 94 elements H-Pu, *The Journal of Chemical Physics*. 132 (2010) 154104–20. doi:10.1063/1.3382344.

- [70] G. Scalmani, M.J. Frisch, Continuous surface charge polarizable continuum models of solvation. I. General formalism, *The Journal of Chemical Physics*. 132 (2010) 114110–16. doi:10.1063/1.3359469.
- [71] P.M. Rudd, A.H. Merry, M.R. Wormald, R.A. Dwek, Glycosylation and prion protein, *Curr. Opin. Struct. Biol.* 12 (2002) 578–586.
- [72] S. Hornemann, C. Schorn, K. Wuthrich, NMR structure of the bovine prion protein isolated from healthy calf brains, *EMBO Rep.* 5 (2004) 1159–1164. doi:10.1038/sj.embor.7400297.
- [73] H. Liu, L. Wang, A. Brock, C.-H. Wong, P.G. Schultz, A Method for the Generation of Glycoprotein Mimetics, *J. Am. Chem. Soc.* 125 (2003) 1702–1703. doi:10.1021/ja029433n.
- [74] H.C. Hang, C.R. Bertozzi, Chemoselective Approaches to Glycoprotein Assembly, *Acc. Chem. Res.* 34 (2001) 727–736. doi:10.1021/ar9901570.
- [75] I.V. Baskakov, E. Katorcha, Multifaceted Role of Sialylation in Prion Diseases, *Front. Neurosci.* 10 (2016) 32–15. doi:10.3389/fnins.2016.00358.
- [76] E. Katorcha, M.L. Daus, N. Gonzalez-Montalban, N. Makarava, P. Lasch, M. Beekes, et al., Reversible off and on switching of prion infectivity via removing and reinstalling prion sialylation, *Nature Publishing Group*. (2016) 1–11. doi:10.1038/srep33119.
- [77] E. Katorcha, N. Makarava, R. Savtchenko, A. d Azzo, I.V. Baskakov, Sialylation of Prion Protein Controls the Rate of Prion Amplification, the Cross-Species Barrier, the Ratio of PrPSc Glycoform and Prion Infectivity, *PLoS Pathog.* 10 (2014) e1004366–12. doi:10.1371/journal.ppat.1004366.
- [78] S. Srivastava, E. Katorcha, M.L. Daus, P. Lasch, M. Beekes, I.V. Baskakov, Sialylation Controls Prion Fate *in Vivo*, *Journal of Biological Chemistry*. 292 (2017) 2359–2368. doi:10.1074/jbc.M116.768010.
- [79] J. Stöckel, J. Safar, A.C. Wallace, F.E. Cohen, S.B. Prusiner, Prion Protein Selectively Binds Copper(II) Ions †, *Biochemistry*. 37 (1998) 7185–7193. doi:10.1021/bi972827k.

- [80] T. Mukai, H. Hoshi, K. Ohtake, M. Takahashi, A. Yamaguchi, A. Hayashi, et al., Highly reproductive *Escherichia coli* cells with no specific assignment to the UAG codon, *Nature Publishing Group*. 5 (2015) 1056–9. doi:10.1038/srep09699.
- [81] J.W. Chin, S.W. Santoro, A.B. Martin, D.S. King, L. Wang, P.G. Schultz, Addition of p-Azido- l-phenylalanine to the Genetic Code of *Escherichia coli*, *J. Am. Chem. Soc.* 124 (2002) 9026–9027. doi:10.1021/ja027007w.
- [82] S. Cao, F.D. Tropper, R. Roy, Stereoselective phase transfer catalyzed syntheses of glycosyloxysuccinimides and their transformations into glycoprobes, *Tetrahedron*. 51 (1995) 6679–6686. doi:10.1016/0040-4020(95)00325-3.
- [83] C. Wiedemann, P. Bellstedt, M.G. Bioinformatics, 2013, CAPITO—a web server-based analysis and plotting tool for circular dichroism data, *Academic.Oup.com*. (n.d.). doi:10.1142/S0218810417500186.
- [84] J.R. Piro, B.T. Harris, K. Nishina, C. Soto, R. Morales, J.R. Rees, et al., Prion protein glycosylation is not required for strain-specific neurotropism, *J Virol*. 83 (2009) 5321–5328. doi:10.1128/JVI.02502-08.
- [85] R.A. Bessen, D.A. Kocisko, G.J. Raymond, S. Nandan, P.T. Lansbury, B. Caughey, Non-genetic propagation of strain-specific properties of scrapie prion protein, *Nature*. 375 (1995) 698–700. doi:10.1038/375698a0.
- [86] J. Collinge, K.C. Sidle, J. Meads, J. Ironside, A.F. Hill, Molecular analysis of prion strain variation and the aetiology of “new variant” CJD, *Nature*. 383 (1996) 685–690. doi:10.1038/383685a0.
- [87] X. Xiao, J. Yuan, S. Haïk, I. Cali, Y. Zhan, M. Moudjou, et al., Glycoform-selective prion formation in sporadic and familial forms of prion disease, *PLoS ONE*. 8 (2013) e58786. doi:10.1371/journal.pone.0058786.
- [88] E. Cancellotti, S.P. Mahal, R. Somerville, A. Diack, D. Brown, P. Piccardo, et al., Post-translational changes to PrP alter transmissible spongiform encephalopathy strain properties, *The EMBO Journal*. 32 (2013) 756–769. doi:10.1038/emboj.2013.6.

- [89] J. Castilla, R. Morales, P. Saá, M. Barria, P. Gambetti, C. Soto, Cell-free propagation of prion strains, *The EMBO Journal*. 27 (2008) 2557–2566. doi:10.1038/emboj.2008.181.
- [90] R.A. Somerville, Host and transmissible spongiform encephalopathy agent strain control glycosylation of PrP, *J Gen Virol*. 80 (Pt 7) (1999) 1865–1872. doi:10.1099/0022-1317-80-7-1865.
- [91] S.J. DeArmond, Y. Qiu, H. Sánchez, P.R. Spilman, A. Ninchak-Casey, D. Alonso, et al., PrP^{Sc} glycoform heterogeneity as a function of brain region: implications for selective targeting of neurons by prion strains, *J Neuropathol Exp Neurol*. 58 (1999) 1000–1009. doi:10.1097/00005072-199909000-00010.
- [92] T. Kuczius, R. Koch, K. Keyvani, H. Karch, J. Grassi, M.H. Groschup, Regional and phenotype heterogeneity of cellular prion proteins in the human brain, *Eur J Neurosci*. 25 (2007) 2649–2655. doi:10.1111/j.1460-9568.2007.05518.x.
- [93] K.M. Schilling, L. Tao, B. Wu, J.T.M. Kiblen, N.C. Ubilla-Rodriguez, M.J. Pushie, et al., Both N-Terminal and C-Terminal Histidine Residues of the Prion Protein are Essential for Copper Coordination and Neuroprotective Self-Regulation, *Journal of Molecular Biology*. (2020) 1–38. doi:10.1016/j.jmb.2020.05.020.
- [94] K.M. Schilling, N.C. Ubilla-Rodriguez, C.W. Wells, G.L. Millhauser, Production of Artificially Doubly Glycosylated, ¹⁵N Labeled Prion Protein for NMR Studies Using a pH-Scanning Volatile Buffer System, *J. Org. Chem*. 85 (2020) 1687–1690. doi:10.1021/acs.joc.9b02430.